Milky Way satellite velocities reveal the dark matter power spectrum at small scales

Ivan Esteban,[1,2,*] Annika H. G. Peter,[1,2,3,4,†] and Stacy Y. Kim[5,‡]

[1]*Center for Cosmology and AstroParticle Physics (CCAPP), Ohio State University, Columbus, Ohio 43210, USA*
[2]*Department of Physics, Ohio State University, Columbus, Ohio 43210, USA*
[3]*Department of Astronomy, Ohio State University, Columbus, Ohio 43210, USA*
[4]*School of Natural Sciences, Institute for Advanced Study, 1 Einstein Drive, Princeton, New Jersey 08540*
[5]*Department of Physics, University of Surrey, Guildford, GU2 7XH, United Kingdom*

(Received 21 June 2023; accepted 30 October 2024; published 5 December 2024)

Dark matter (DM) properties at small scales remain uncertain. Recent theoretical and observational advances have provided the tools to narrow them down. Here, we show for the first time that the correlation between internal velocities and sizes of dwarf galaxies is a sharp probe of small-scale DM properties. We study modified DM power spectra, motivated by DM production during inflation. Using semianalytic models and scaling relations, we show that such models can change the kinematics and structure of dwarf galaxies without strongly affecting their total abundance. We analyze data from Milky Way classical satellite galaxies and those discovered with the Sloan Digital Sky Survey, finding that the DM power spectrum at comoving scales 4 $\mathrm{Mpc}^{-1} < k < 37\ \mathrm{Mpc}^{-1}$ cannot deviate by more than a factor of ∼2.5 from scale invariance. Our results are robust against baryonic uncertainties such as the stellar mass-halo mass relation, halo occupation fraction, and subhalo tidal disruption; allowing us to independently constrain them. This work thus opens a window to probe both dwarf galaxy formation models and small-scale DM properties.

DOI: 10.1103/PhysRevD.110.123013

I. INTRODUCTION

Dark matter (DM) is the second most abundant component of the Universe, yet its nature remains mysterious. At scales well above the size of a galaxy, observations are compatible with a cold, collisionless particle [1–3]: the Cold Dark Matter (CDM) paradigm. At smaller scales, this paradigm has been challenged in the past by discrepancies between simulations and observations [4–7].

These "small-scale" tensions have sparked interest in DM models that may alleviate them by affecting structure formation at galactic and subgalactic scales [8–11]. Even if baryonic physics and improved observations may also alleviate them [4,5,7,12], the interest of modified DM models is broader, as they provide a framework to characterize the properties of DM. Theoretical and observational techniques developed to understand these tensions are then an effective tool to establish the nature of DM. Previous work used Milky Way satellite luminosities [13–21] and stellar velocity dispersions [21,22] to constrain the DM particle mass and interactions.

In this paper, we develop a powerful observable to determine small-scale DM properties: a joint constraint of the internal velocity, size, and total abundance of dwarf galaxies. Using semianalytic techniques and scaling relations, inspired by physics models and calibrated against simulations, we show that the correlation between these

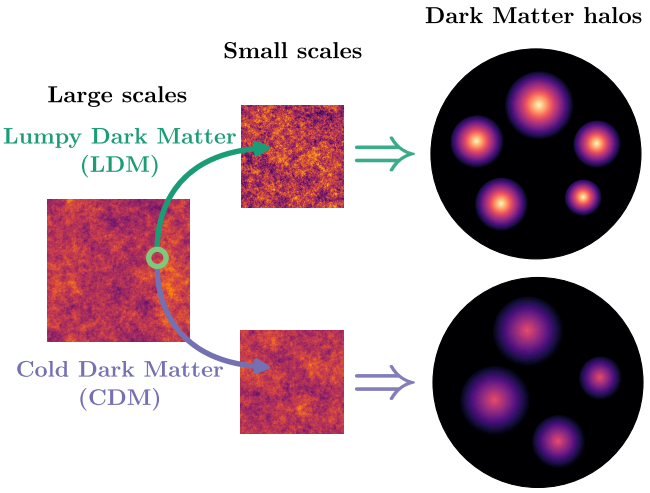

FIG. 1. Depiction of Lumpy Dark Matter models, generated with CMBPY [33]. Due to the enhanced power at small scales, in such models halos are more dense and abundant than in CDM.

*Contact author: esteban.6@osu.edu
†Contact author: peter.33@osu.edu
‡Contact author: s.kim@surrey.ac.uk

properties contains information on DM physics that can be disentangled from galaxy formation uncertainties. We perform a statistical analysis of classical and SDSS Milky Way dwarfs, and quantify the agreement with CDM.

The method broadly applies to DM models with modified structure formation or primordial power spectra [8–11,23,24]. In this first paper, we mainly focus on models with enhanced structure at small scales. This is a natural prediction if DM is produced out of quantum fluctuations during inflation [25–27]. Even if these models do not require nongravitational interactions between DM and baryons, limiting the detectability of DM in the laboratory, DM being produced out of small-scale isocurvature fluctuations entails significant substructure that may be tested. Similar effects are also predicted by primordial magnetic fields [23] or in nonstandard inflationary models [24,28,29]. Because of the enhanced substructure, we name these DM models *Lumpy Dark Matter (LDM)*.

Figure 1 previews the big picture. LDM models resemble CDM on large scales, but on small scales density fluctuations are greater. Hence, when these fluctuations collapse to form DM halos, the larger fluctuation amplitudes in LDM result in more halos than in CDM. LDM halos also form earlier, when the Universe is denser, so their internal densities are higher. Our analysis probes both the increased abundance and densities, allowing us to *determine the DM power spectrum with good precision at small scales*, where to our knowledge only strong lensing determinations exist [30]. As usual in the literature, in this first study we use semianalytic techniques [28,30–32]. Future work could improve on these results using simulation-based inference, ideally including baryons.

Quantitatively, LDM models are characterized by an enhanced primordial curvature power spectrum at small scales, that we parametrize as

$$\mathcal{P}_{\mathcal{R}}(k) \propto k^{n_s-1}[1+(k/k_{\rm cut})^{n_{\rm cut}-n_s}], \tag{1}$$

with k comoving wavenumber, $n_s \simeq 0.97$ the standard CDM spectral index [1], $k_{\rm cut}$ the comoving wavenumber above which power is enhanced, and $n_{\rm cut} > n_s$ the enhanced spectral index. This expression interpolates from $\mathcal{P}_{\mathcal{R}} \propto k^{n_s-1}$ at $k \ll k_{\rm cut}$ to $\mathcal{P}_{\mathcal{R}} \propto k^{n_{\rm cut}-1}$ at $k \gg k_{\rm cut}$. Perturbations evolve as in CDM [25–27].

LDM models are phenomenologically interesting because, in contrast to most of the modified DM models studied in the literature [8–11], the DM power spectrum is enhanced instead of suppressed. This opens new observational effects and channels with which to test them. In addition, some datasets suggest a "too many satellites" problem [16,34,35] that might point to such models.

The rest of the paper is organized as follows. Section II quantifies the impact of LDM models on DM halo properties. Section III links to the properties of dwarf galaxies, discusses baryonic effects, and shows that the correlation between galaxy kinematics and size is a sharp probe of DM substructure. Section IV describes our statistical analysis and results, and comments on suppressed power. Section V concludes and points out future research directions. The Appendices provide further details.

Below, we assume a Planck 2018 cosmology [1] ($h = 0.67, \Omega_{\rm m} = 0.31, \sigma_8 = 0.81, \Omega_\Lambda = 0.69, \Omega_{\rm b} = 0.05$). We carry out DM calculations with the `Galacticus` [36] semianalytic halo formation code. Unless otherwise specified, we evaluate Milky Way satellite properties at median infall redshift $z_{\rm infall} = 1$ [37–39], i.e., when entering the Milky Way virial radius. We define halo virial masses as M_{200c}, i.e., the mean overdensity within the virial radius relative to the critical density is $\Delta = 200$. We assume a Milky Way mass of $10^{12} M_\odot$ and concentration of 9 [40]. We comment on these choices in Sec. III.

II. IMPACT ON DWARF GALAXY HALOS

In this section, we use semianalytic techniques to compute the impact of LDM models on DM halos. We show that enhanced power at small scales increases the number of low-mass halos and their central densities, leading to unique observational signatures in dwarf galaxies.

A. Formalism

We follow the extended Press-Schechter formalism [41,42], which assigns DM halos to regions where density perturbations exceed a threshold. This formalism is expected to hold for a wide range of power spectra and cosmological models [43,44], and connects DM halos to the power spectrum through the variance of the density field

$$\sigma^2(R(M),z) \equiv \int \frac{{\rm d}^3k}{(2\pi)^3} P_{\rm lin}(k,z)|W(k,R)|^2, \tag{2}$$

where $R(M) \equiv [3M/(4\pi\bar{\rho}_m)]^{1/3}$ is the Lagrangian radius of the halo with M its mass and $\bar{\rho}_m$ the average matter density of the Universe, z is redshift, $P_{\rm lin}$ is the linear matter power spectrum, and $W(k,R)$ is a window function that connects the comoving wavenumber to Lagrangian radius. To avoid spurious halos at scales larger than those with enhanced power, we use a sharp k-space window [44]

$$W(k,R) = \theta(2.5/R - k), \tag{3}$$

with θ the step function. Different window functions do not significantly change the results [45].

The number density of halos per unit mass, i.e., the halo mass function, is then

$$\frac{{\rm d}n_{\rm halo}}{{\rm d}M} = f(\sigma,z)\frac{\bar{\rho}_m}{M}\left|\frac{{\rm d}\log\sigma(R(M),z)}{{\rm d}M}\right|. \tag{4}$$

We use the Sheth-Tormen mass function f that extends the Press–Schechter formalism to ellipsoidal collapse [46]

$$f(\sigma, z) = A[1 + (a\nu)^{-p}]\sqrt{a}e^{-a\nu/2}/\sqrt{2\pi\nu}, \quad (5)$$

where $\nu \equiv \delta_c/\sigma$ with δ_c the linear overdensity threshold for spherical collapse; and A, a, and p are parameters calibrated to simulations. This formalism reproduces simulations with modified power spectra [47–49], and CDM simulations down to halo masses $M \sim 10^7 M_\odot$ [50]. Lower-mass halos are not expected to host galaxies and hence are not relevant for our analysis (see Sec. III A). We set $\delta_c = 1.686$, corresponding to an Einstein–de Sitter universe; and $A = 0.30$, $a = 0.79$, and $p = 0.22$ [51]. As we are interested in Milky Way satellites, we need the *subhalo* mass function, which we compute following the merger tree algorithm from Refs. [52–54]. This algorithm describes the hierarchical formation history of DM halos. As we show below, our results do not strongly rely on the halo mass function, so potential uncertainties related to the extended Press–Schechter formalism in LDM models are subdominant contributions to our error budget. We include an overall 20% suppression of the subhalo mass function due to baryons across all relevant masses ($M < 10^{11} M_\odot$; see below) [55–58].

We also explore halo density profiles. For low-mass halos, we assume a Navarro-Frenk-White (NFW) form [59]

$$\rho(r) = \frac{\rho_s}{r/r_s(1 + r/r_s)^2}, \quad (6)$$

with ρ_s a characteristic density and r_s the scale radius. For higher-mass halos, we include baryonic feedback by making the profiles cored as we describe in Sec. III A. We parametrize r_s in terms of the concentration

$$c_{200c} \equiv r_{\rm vir}/r_s, \quad (7)$$

with $r_{\rm vir}$ the virial radius. For fixed mass, halos with larger concentrations have larger central densities.

As already discussed in the original NFW paper, there is a correlation between halo concentration and formation time that generates a mass-concentration relation. *Halos formed at higher redshift have higher concentrations at the present, reflecting that the average matter density of the Universe was larger at formation* [59–62]. This correlation was studied in detail by Diemer and Joyce [62], who proposed a semianalytic relation between concentration, mass, power-spectrum slope, and formation redshift, not tuned to any specific cosmology or redshift range. This was shown to accurately reproduce the results of N-body simulations for a variety of masses, redshifts, and power spectra (see also Ref. [63]). Hence, we adopt the mass-concentration relation from Ref. [62]. When computing concentrations, we include a lognormal scatter of 0.16 dex [64]; i.e., we assume that halo concentration follows a lognormal distribution with a median given by the relation in Ref. [62] and a standard deviation of 0.16 dex.

B. Consequences

The impact of enhanced power spectra on halo properties is now more explicit. From Eq. (2), enhanced power increases the variance of the density field σ, which leads to *enhanced halo abundances*; see Eqs. (4) and (5). Halos also form earlier, as can be understood from the collapsed mass fraction in extended Press–Schechter theory [61,65],

$$M_{\rm coll}(z) = M_0 \,{\rm erfc}\left(\frac{\delta_c/[\sqrt{2}(1 - D(z_0)/D(z))]}{\sqrt{\sigma^2(fM_0, z) - \sigma^2(M_0, z)}}\right), \quad (8)$$

with $M_{\rm coll}$ the mass of halo progenitors more massive than fM_0 that have collapsed by redshift z, $M_0 \equiv M(z_0)$ the final halo mass, and $D(z)$ the linear growth factor. As $M_{\rm coll}(z)$ is a growing function of σ, enhanced power leads to early halo formation and *high concentrations* [28,48].

Below, we quantify both effects and show that the impact on halo concentrations is more dramatic. This can greatly affect the kinematics of galaxies inhabiting them.

Figure 2 shows that LDM models can significantly affect the internal halo kinematics due to the enhanced concentrations. For LDM, we set $k_{\rm cut} = 8$ Mpc^{-1} and $n_{\rm cut} = 2.6$ (our analysis below excludes this). The top-right panel shows the redshift of halo formation computed following

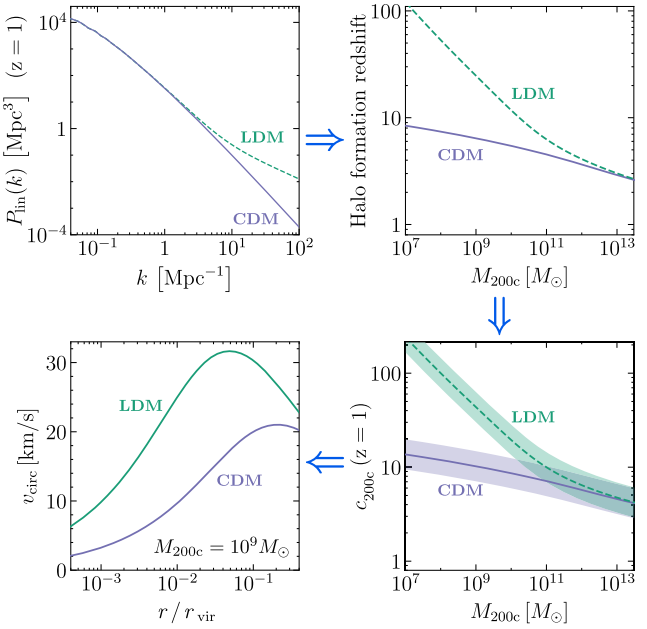

FIG. 2. Impact of LDM models on halo structure. An enhanced power spectrum (top left) leads to early halo formation (top right), when the DM density is higher, leading to more concentrated halos (bottom right, shaded regions represent 1σ scatter) and higher internal velocities (bottom left).

Ref. [61], defined as the redshift at which the mass within r_s was contained in halo progenitors more massive than 2% of the final halo mass. The bottom-right panel shows halo concentrations computed following Ref. [62] as described above, along with 0.16 dex scatter [64]. The bottom-left panel shows the circular velocity curve, $v_{\rm circ}(r) = \sqrt{GM(<r)/r}$ with G Newton's constant, $M(<r)$ the enclosed mass, and r radius (for fixed halo mass and an NFW profile). Other halos are similarly affected, but in a mass- and model-dependent way. These plots do not include tidal stripping or baryonic effects that we introduce in Sec. III A.

The results in Fig. 2 quantify the effects described above. If power is enhanced below a given scale, halos below a given mass will form earlier. This leads to large concentrations, i.e., large DM densities close to the halo center, implying large circular velocities.

A fortuitous cancellation increases the impact of modified power on the mass-concentration relation. For the currently favored nearly scale-invariant power spectrum, at small scales $P_{\rm lin}(k) \propto k^{-3}$ approximately [66]. The integrand in Eq. (2) is then proportional to k^{-1}, and $\sigma(R)$ only grows logarithmically with $1/R$: at small scales $\sigma(R)$ "flattens out," all halos form at similar redshifts, and thus have similar concentrations. Deviations from scale invariance such as those we consider induce a stronger dependence of σ on R, greatly increasing the differences in formation time and concentration between halos.

Figure 3 shows that visible subhalo abundance is not much enhanced in the LDM models we explore. We show the $z = 0$ subhalo mass function for a parent halo with Milky Way mass, computed with `Galacticus` following Refs. [52–54] as described above. We use the same LDM parameters as in Fig. 2, $k_{\rm cut} = 8$ Mpc^{-1} and $n_{\rm cut} = 2.6$. The background shows the halo occupation fraction, i.e., the probability for a DM halo to host a galaxy, from Ref. [38] (when performing our data analysis below, we set this free). M_{200c} is the subhalo mass at infall; we discuss tidal effects and subhalo disruption in Sec. III A.

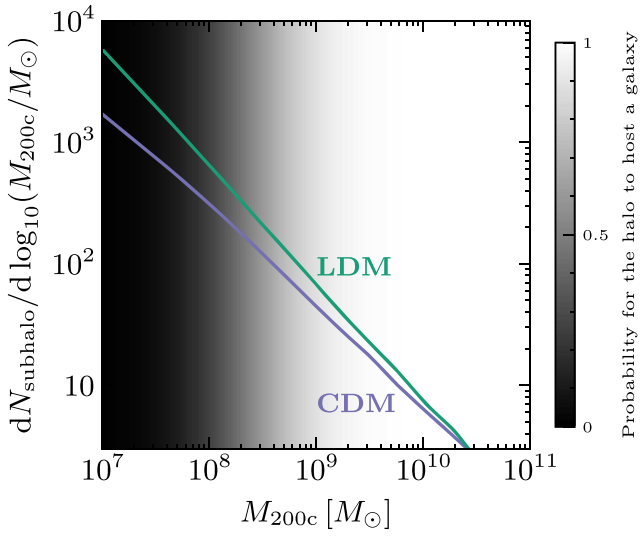

FIG. 3. Impact of LDM models on the subhalo mass function. The grayscale shows the probability for halos to host galaxies in an illustrative model (we later set this free; see the text). The models we explore marginally affect visible subhalo abundance; our main observable is the enhanced concentrations.

The largest impact of LDM on halo abundances is on halos that are not expected to host galaxies: the subhalo mass function differs from CDM by ∼35% at $10^9 M_\odot$ and by ∼50% at $10^8 M_\odot$. Thus, our main observable is not total halo abundance, which we include for completeness and to lift degeneracies, but internal halo properties.

Overall, we conclude that LDM models strongly affect central densities of low-mass halos. Any kinematic probe of the inner part of such halos is thus a sensitive probe of LDM models. In the following, we follow the procedure in Ref. [22], extending the code `dis` [67] to predict and observationally probe Milky Way satellite circular velocities and sizes, linking them to the DM power spectrum.

III. IMPACT ON MILKY WAY SATELLITES

In this section, we link low-mass DM halo properties to dwarf galaxy properties. We show that enhanced power predicts a characteristic relation between stellar kinematics and galaxy size that can be observationally explored.

As mentioned in Sec. I, we fix the Milky Way mass to $10^{12} M_\odot$ and evaluate satellite properties at median infall redshift. As we show in Appendices A and B, the impact of leaving these free in our analysis is negligible, as other free parameters dominate our error budget. We also neglect specific aspects of the Milky Way merger history, like the Magellanic Clouds. Although recent work shows that they impact satellite counts [68–72], the effect is smaller than our overall error budget (see Appendix B). In addition, we use satellites discovered by SDSS, whose footprint does not contain the Magellanic Clouds (see Ref. [73]). If other constraints improve in future work, or if satellites recently discovered in the Southern Hemisphere are included [74–86], this may need revisiting.

A. Formalism

It is challenging to directly observe low-mass DM halos. Avenues include gravitational lensing [34], already quite mature (see, e.g., Refs. [87–92]); perturbations to the Milky Way stellar disk [93,94]; or disruption of stellar streams [95–97]. These may probe halos smaller than those that host galaxies. Yet observing the dwarf galaxies that low-mass halos host provides unique access to their central regions. This, as shown above in Fig. 2, is a sharp probe of LDM models. Dwarf galaxies are also DM dominated [98,99], alleviating baryonic uncertainties that are more significant for more massive galaxies.

Below, we describe how we use the output from `Galacticus` (subhalo masses, concentrations, and total abundance) to build a Milky Way satellite galaxy population. To probe the central kinematics affected by LDM models, we need to predict the relationship among galaxy sizes, internal velocities, and observational abundance.

We quantify galaxy size by its 2D-projected half-light radius [22], that we denote as $R_{\rm eff}$. It is correlated with its stellar mass M_* by an empirical scaling relation,

$$\log_{10}(R_{\rm eff}/{\rm kpc}) = 0.268\log_{10}(M_*/M_\odot) - 2.11. \quad (9)$$

This relation has 0.234 dex lognormal scatter. It was obtained in Ref. [22] using isolated dwarf data [100,101], and it is similar to the relation found for satellites in the Local Group [102] and in simulations [103]. Although this relation can have uncertainties at low $R_{\rm eff}$ due to selection effects related to surface brightness, these effects impact faint galaxies with a very low observation probability (see below), which are a subdominant sample in our analysis (see also Appendix B).

The stellar mass M_*, in turn, links to the infall halo mass [104] M_{200c} via the stellar mass-halo mass relation, that we parametrize as a power law

$$M_* = M_{200c}\mathcal{N}\left(\frac{M_{200c}}{M_0}\right)^{\beta^{M_*}}, \quad (10)$$

with $\mathcal{N}$ a constant, M_0 a reference mass, and β^{M_*} the power-law slope. At dwarf galaxy masses this relation is poorly constrained, and most relations are calibrated at higher mass and then extrapolated [38,104–106] (see, however, Refs. [71,73,107]). At $z = 1$, Ref. [104] found $\mathcal{N} = 0.046$, $M_0 = 1.5\times10^{12}M_\odot$, and $\beta^{M_*} = 0.96$. The scatter in this relation is also uncertain and potentially mass dependent [106,108–110]; we parametrize it as

$$\sigma(M_*) = \sigma^{M_*} + \gamma^{M_*}\log_{10}\frac{M_{200c}}{10^{11}M_\odot}{\rm dex}. \quad (11)$$

In our data analysis below, we set β^{M_*}, σ^{M_*}, and γ^{M_*} to be free parameters. This also allows us to observationally explore the low-mass stellar mass-halo mass relation.

We quantify internal velocity by the line-of-sight stellar velocity dispersion $\sigma^*_{\rm los}$. We use the estimator from [111]

$$\sigma^*_{\rm los} = \sqrt{\frac{G}{4}\frac{M(<r_{1/2})}{R_{\rm eff}}}, \quad (12)$$

with $M(<r_{1/2})$ the mass enclosed by the 3D half-light radius $r_{1/2} = R_{\rm eff}/0.75$ (this is accurate for a wide variety of stellar distributions [111]). Other estimators produce very similar results [22]; see Appendix A. $M(<r)$ only includes DM, as the stellar mass is subdominant [98,99].

$\sigma^*_{\rm los}$ links to halo concentration through the density profile entering $M(<r)$, which can be affected by baryonic feedback that turns central NFW "cusps" predicted by DM-only simulations into "cores" [112–121] (this is expected to happen at halo masses $M \lesssim 10^8$–10^{10}, although there are large uncertainties [22,122–124]). We include this effect by setting cored profiles above a threshold halo mass $M^{\rm core}_{\rm thres}$. We use the simulation- and observation-constrained profile from Ref. [124], where the core size depends on the time over which a galaxy has formed stars, assuming that satellites stop forming stars at infall. $M^{\rm core}_{\rm thres}$ is uncertain, so in our data analysis below we set it to be a free parameter. This allows us to observationally explore the cusp-core transition.

The Milky Way gravitational field can tidally strip DM subhalos, changing their density profile (we discuss tidal disruption at the end of this section). This may be modeled by truncating the density profile beyond the tidal radius [30,91,125], defined as the radius where the Milky Way tidal force balances the attractive force of the subhalo [126], and by modifying structural halo parameters due to tidal shocking and heating [127–134]. Importantly for this study, as we demonstrate in Appendix A (Fig. 9), only when the *average mass loss* of the satellite population is $\gtrsim$99% are our results affected (our population study is sensitive to *average* properties). Though uncertain, the average mass loss of undisrupted Milky Way satellites is estimated to be ∼30%–90% [110,135–138]. Hence, tidal stripping is a minor contribution to our error budget and we do not include it in our main results. Physically, this is because our observables are sensitive to halo properties inside the half-light radius, usually smaller than the tidal radius; and because galaxies remain unaffected until their DM halos lose more than 90% of their mass [22,139,140]. The high concentrations of LDM halos may also make them more resilient to tidal stripping [129,141]; further work is needed to assess this.

Regarding observational abundance, not all DM halos are expected to host galaxies. Only those more massive than 10^7–$10^8M_\odot$ by reionization would have gas that can cool and form stars [142–144]. We include this via the halo occupation fraction, i.e., the probability for a halo to host a galaxy, that we parametrize as a sigmoid function

$${\rm hof}(M_{200c}) = \frac{1+{\rm erf}(\alpha^{\rm hof}\log_{10}[M_{200c}/M_0^{\rm hof}])}{2}, \quad (13)$$

with erf the error function, $M_0^{\rm hof}$ the mass below which halos do not host galaxies, and $\alpha^{\rm hof}$ a parameter controlling the steepness of the transition. With simulation and semi-analytic modeling, Refs. [38,145] found $\alpha^{\rm hof} = 1.3$ and $M_0^{\rm hof} = 10^{8.4}M_\odot$; there are also observational limits from the Milky Way satellite luminosity function [17,71]. In our data analysis below, we set $\alpha^{\rm hof}$ and $M_0^{\rm hof}$ to be free parameters. This allows us to observationally determine the low-mass halo occupation fraction.

Not all halos hosting galaxies are observable either: for a given survey, faint and distant galaxies will escape detection. We account for this by assigning to each galaxy with stellar mass below $4\times10^5 M_\odot$ (brighter galaxies correspond to classical satellites) an observation probability

$$\mathcal{P}_{\rm obs}=\frac{\int_{V_{\rm obs}(L)} n(\vec{r})\mathrm{d}^3 r}{\int_{V_{\rm vir}} n(\vec{r})\mathrm{d}^3 r}\equiv\frac{1}{\mathcal{C}(L)}, \tag{14}$$

with n the number density of satellites, $V_{\rm vir}$ the Milky Way virial volume, and $V_{\rm obs}(L)$ the volume where satellites with luminosity L can be detected by the survey. $\mathcal{C}(L)$ is the luminosity-dependent completeness correction [16]. We compute luminosities assuming $M_*/M_\odot=2L/L_\odot$, appropriate for old stellar populations [111,146].

A priori, $\mathcal{P}_{\rm obs}$ depends both on L and $R_{\rm eff}$ [73,147], but the latter dependence can be absorbed through the empirical $R_{\rm eff}$–M_* relation of observed galaxies [148], producing an *effective* $\mathcal{P}_{\rm obs}$ that only depends on L. Uncertainties on that relation do not significantly affect our error budget; see Appendix B. In short, uncertainties impact galaxies with very low observation probability, so our choices are appropriate to predict the population of SDSS-like galaxies. In addition, uncertainties can be partly absorbed in the stellar mass-halo mass relation and halo occupation fraction that we set free.

We assume that $n(\vec{r})$ does not change significantly with the solid angle, so that the selection function is separable into a radial and an angular component

$$\mathcal{C}(L)\equiv\mathcal{C}_\Omega\mathcal{C}_r;\quad \mathcal{C}_\Omega\equiv\frac{4\pi}{\Omega};\quad \mathcal{C}_r\equiv\frac{\int_0^{r_{\rm vir}} n(r)r^2\mathrm{d}r}{\int_0^{r_{\rm c}(L)} n(r)r^2\mathrm{d}r}, \tag{15}$$

with Ω the angular coverage of the survey, $r_{\rm vir}$ the Milky Way virial radius, and $r_{\rm c}(L)$ the largest distance at which satellites of luminosity L can be observed by the survey. We consider classical and SDSS satellites; for the latter $\Omega_{\rm SDSS}=3.65$ sr and $r_{\rm c}$ is given by [147,148]

$$r_{\rm c}(L)=1.5\ \mathrm{kpc}\ (L/L_\odot)^{0.51}. \tag{16}$$

$\mathcal{C}_\Omega$ has 19% scatter due to anisotropy [13]. As mentioned above, we neglect the impact of the Magellanic Clouds on anisotropy [73,86], because the SDSS footprint does not include them; and extra scatter of $\mathcal{C}_\Omega$ would only affect the total number of satellites that is not our main observable and has already a large error (see Appendix B).

The Milky Way can also tidally disrupt DM halos. This would remove galaxies from our sample and affect the radial distribution of undisrupted satellites $n(r)$, which is hence very uncertain [16,57,58,110,149–155]. This made it a big systematic uncertainty in previous work of satellite populations [16,71]. To be conservative, we are agnostic about tidal disruption and include both effects by parametrizing $n(r)$ as

$$n(r)=n_{\rm GK17}(r)+y_{\mathcal{C}}[n_{\rm NFW}(r)-n_{\rm GK17}(r)], \tag{17}$$

with $y_{\mathcal{C}}\in[0,1]$ a parameter that interpolates between an unstripped NFW distribution, $n_{\rm NFW}(r)$—i.e., satellites follow the DM halo distribution, and the strongly disrupted distribution from Ref. [149], $n_{\rm GK17}(r)$ (named `FIRE` in Ref. [149]; see also the dotted line in Fig. 1 of Ref. [16]). In our analysis below, we set $y_{\mathcal{C}}$ free, which allows us to observationally explore tidal subhalo disruption.

B. Consequences

Figure 4 illustrates how the large concentrations predicted in LDM models get imprinted on galaxies in the form of high stellar velocity dispersions, which can be in tension with Milky Way satellite data. We plot the correlation between $\sigma^*_{\rm los}$ and $R_{\rm eff}$ of Milky Way satellites. We generate the theoretical expectations by sampling halo masses from the product of the subhalo mass function described in Sec. II A and the halo occupation fraction from Ref. [38], and sampling halo concentrations as described in Sec. II A. We use the same LDM parameters as in Figs. 2 and 3, $k_{\rm cut}=8\ \mathrm{Mpc}^{-1}$ and $n_{\rm cut}=2.6$ (our analysis below excludes this). We assign $R_{\rm eff}$ and $\sigma^*_{\rm los}$ using Eqs. (9) and (12). $R_{\rm eff}$ depends on the stellar mass that we generate using the stellar mass-halo mass relation from Ref. [104] with lognormal scatter of 0.15 dex [104]. $\sigma^*_{\rm los}$ depends on the halo density profile: we set cored profiles for halo masses above $M^{\rm core}_{\rm thres}=10^9 M_\odot$ [22]. Finally, we weight

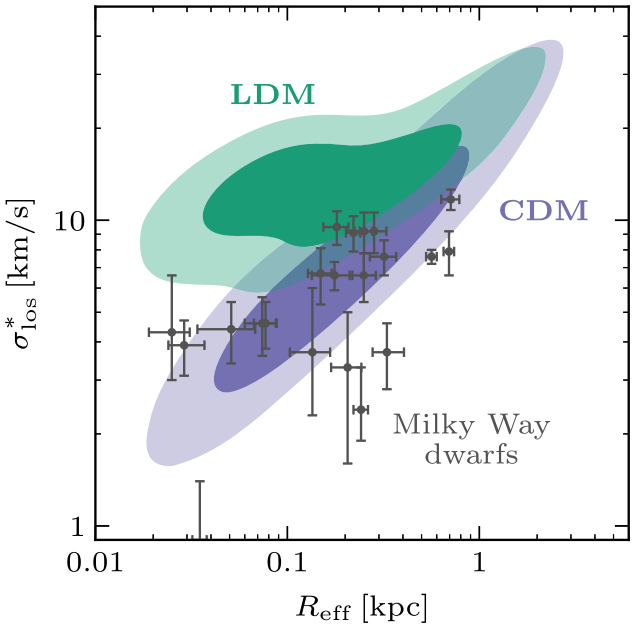

FIG. 4. Correlation between stellar velocity dispersion and half-light radius, and data from classical and SDSS Milky Way dwarfs. Colored regions enclose 68% and 95% of the predicted population, for an illustrative model connecting halos to galaxies (see Sec. III B; we later set this free). Data disfavors the high velocity dispersions of LDM models.

each galaxy by its observation probability $\mathcal{P}_{\rm obs}$, computed with Eq. (14) for an undisrupted NFW spatial distribution of satellites [i.e., $y_{\mathcal{C}} = 1$ in Eq. (17)]. Data correspond to classical and SDSS satellites, as obtained from Refs. [22,100,156] and compiled in Appendix D. In our analysis below, we allow the parameters of the stellar mass-halo mass relation, the halo occupation fraction, the halo mass where baryonic feedback switches the profiles from NFW to cored, and the amount of tidal subhalo disruption to vary; this significantly affects the predicted population (see Appendix A). It also increases the agreement of data with CDM, although our choices for Fig. 4 are within the 2σ allowed region (see Appendix C).

As we see from Fig. 4, velocity dispersion $\sigma^*_{\rm los}$ is correlated with half-light radius $R_{\rm eff}$. Galaxies with low $R_{\rm eff}$ are less massive [see Eqs. (9) and (10)], which leads to lower $\sigma^*_{\rm los}$ [see Eq. (12)]. However, $\sigma^*_{\rm los}$ also depends on the central density, i.e., on the halo concentration. As in LDM models low-mass halos have higher concentrations than in CDM; LDM predicts higher $\sigma^*_{\rm los}$ at low $R_{\rm eff}$.

These results highlight that *taking into account stellar kinematics and their correlation with the half-light radius is a powerful observational probe of the DM power spectrum*. Below, we carry out a statistical analysis of classical and SDSS Milky Way satellites to quantify this.

IV. STATISTICAL ANALYSIS AND RESULTS

The procedure described above allows us to predict the number of visible Milky Way satellites, as well as their line-of-sight stellar velocity dispersions $\sigma^*_{\rm los}$ and half-light radii $R_{\rm eff}$, for CDM and LDM models. In this section, we use observational data to infer the primordial DM power spectrum and the galaxy-halo connection parameters.

We fit the number of classical and SDSS Milky Way satellites, their velocity dispersions, and half-light radii—as obtained from Refs. [22,100,156] and compiled in Appendix D; using an unbinned likelihood described in Appendix B. We generate theoretical predictions with `Galacticus`, for DM halo properties, and `dis` for galaxy properties, as described in Secs. II and III. Our free parameters are $\{k_{\rm cut}, n_{\rm cut}\}$, that describe the DM power spectrum $\{\beta^{M_*}, \sigma^{M_*}, \gamma^{M_*}, \alpha^{\rm hof}, M_0^{\rm hof}, M_{\rm thres}^{\rm core}\}$, that describe the galaxy-halo connection; and $y_{\mathcal{C}}$, that parametrizes tidal disruption of Milky Way subhalos. Since the anisotropy of the satellite distribution has 19% scatter [13], we multiply $\mathcal{C}_\Omega$ in Eq. (15) with a free parameter $\sigma_{\mathcal{C}_\Omega}$ and we add a Gaussian prior on $\sigma_{\mathcal{C}_\Omega}$ centered at 1 and with a width of 0.19. $\sigma_{\mathcal{C}_\Omega}$ is our last free parameter.

We perform a frequentist profile-likelihood analysis to avoid prior dependence and Bayesian volume effects. We expect these effects because some parameters are not strongly constrained, there are nontrivial correlations, and part of the parameter space is unbounded.

A. Galaxy properties

Our analysis constrains the relation between galaxies and DM halos with minimal assumptions on baryonic physics and the small-scale DM power spectrum. Below, we describe our inferences on the stellar mass-halo mass relation, the halo occupation fraction, and the amount of subhalo tidal disruption by the Milky Way. We provide the full results of the analysis in Appendix C.

Figure 5 shows the stellar mass-halo mass relation allowed by our analysis within 2σ, compared against observational constraints using the luminosity function [73] (which includes DES and PS1 satellites on top of SDSS and classical satellites, assumes a standard CDM power spectrum, and uses a model for galaxy luminosity and halo occupation fraction), and the extrapolated predictions from the simulation of Ref. [104]. Since we describe the stellar mass-halo mass relation in terms of three parameters—the median power-law slope, the scatter at $10^{11} M_\odot$, and the growth of scatter at low mass; see Eqs. (10) and (11)—and we find significant correlations (see Appendix C), we show the allowed relation for two fixed values of the scatter at $10^{11} M_\odot$: 0.1 dex and 1 dex. Other parameters, including those controlling the DM power spectrum, are allowed to vary freely.

Our median results are compatible with extrapolation from simulation [104]. We see that the median power-law slope is strongly correlated with scatter: if scatter is high, the median stellar mass of low-mass halos has to be small. Otherwise, too many visible satellite galaxies would be predicted. This allows us to obtain a quite robust upper limit on the largest stellar mass of low-mass halos, consistent with previous work [73].

The smallest stellar mass of low-mass halos, however, is worse constrained by our analysis. This is because decreasing the stellar mass would predict less visible satellites, which is partly degenerate with increased halo occupation fraction. *A priori* information on the halo occupation fraction (as in Ref. [73]) would break this degeneracy; we comment on this in the Conclusions.

We also conclude that *the uncertain stellar mass-halo mass relation should not strongly affect our determination of the DM power spectrum*. The main observable for the stellar mass-halo mass relation is the number of observed satellites, whereas the power spectrum is determined mainly from the correlation between stellar velocity dispersion and half-light radius; see Fig. 4. There is only a mild degeneracy because by making low-mass halos brighter, the average velocity dispersion in LDM models can be somewhat reduced. The correlations in our full analysis in Appendix C confirm this intuition.

Figure 6 shows the halo occupation fraction allowed by our analysis within 2σ, together with existing constraints using the luminosity function [71] (using DES and PS1 dwarfs and assuming a standard CDM power spectrum), and the relation inferred in Refs. [38,145] by combining simulation with semianalytic modeling (see also

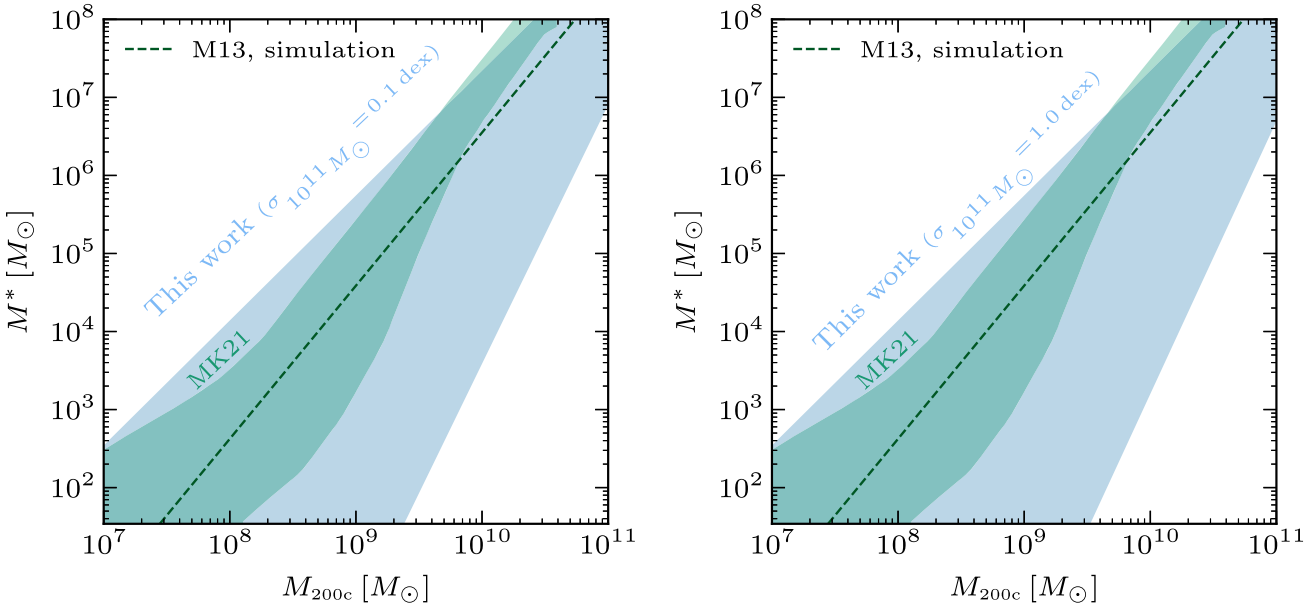

FIG. 5. Stellar mass-halo mass relation allowed by our analysis within 2σ, for different fixed scatters at high mass, together with the simulation prediction that we use in Fig. 4 (Moster *et al.* 2013, M13 [104]) and previous constraints (Manwadkar and Kravtsov 2021, MK21 [73]). Increased scatter suppresses the median stellar mass to avoid overproducing bright galaxies. The lower mass end is degenerate with the halo occupation fraction and is hence more uncertain.

Refs. [17,106]). All the region within the arrows is allowed. Other parameters, including those controlling the DM power spectrum, are allowed to vary freely.

We observe that data requires halos with masses between $10^8 M_\odot$ and $10^{10} M_\odot$ to host galaxies. This is consistent with the results from recent simulations and the luminosity function: if these halos did not host galaxies, there would be a "too many satellites" problem. Our analysis cannot robustly decide if lower-mass halos have a nonzero probability of not hosting galaxies (i.e., if their halo occupation fraction is not 0), as this is degenerate with a modified stellar mass-halo mass relation: very low mass halos can host galaxies if they are very dim.

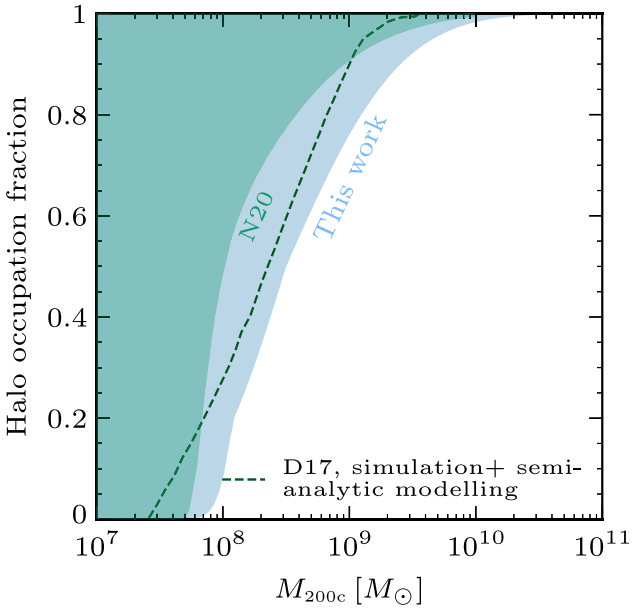

FIG. 6. Halo occupation fraction allowed by our analysis within 2σ, the prediction used in Fig. 4 (Dooley *et al.* 2017, D17 [38]), and previous constraints (Nadler *et al.* 2020, N20 [71]). Regions within the arrows are allowed. Our analysis informs on halo occupation at masses above $\sim 10^8 M_\odot$.

In our analysis, the halo occupation fraction is mildly degenerate with the DM power spectrum, as by populating low-mass halos the average velocity dispersion in LDM models can be reduced. However, the additional handle from the total number of galaxies together with the different correlation between $\sigma^*_{\rm los}$ and $R_{\rm eff}$ in LDM and CDM models (see Fig. 4) alleviate this effect.

Regarding tidal subhalo disruption and the radial satellite distribution in Eqs. (14), (15), and (17), we find $y_C \gtrsim 0.4$ at 1σ (see Appendix C). I.e., our analysis disfavors strong tidal disruption found in simulation [149], as that would produce a "too many satellites" problem [16].

B. Dark matter properties

We now turn to the original purpose of this paper: *what do Milky Way satellite properties tell us about the DM power spectrum at the smallest scales*?

Figure 7 shows that the DM power spectrum cannot be strongly enhanced at dwarf galaxy scales. The allowed parameter space is unbounded because very large $k_{\rm cut}$ is indistinguishable from scale invariance, but our analysis limits how large enhancements can be between comoving

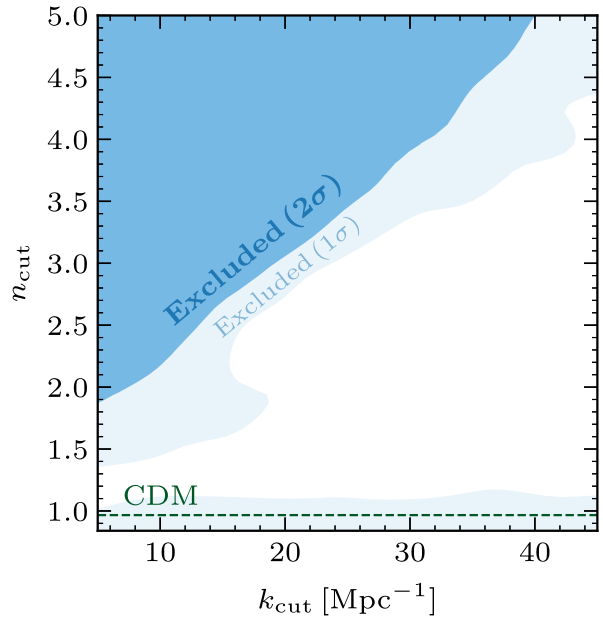

FIG. 7. Excluded values of LDM parameter space in our analysis. Dwarf galaxy velocity dispersions and sizes probe dark matter substructure for 5 Mpc$^{-1} \lesssim k \lesssim 40$ Mpc^{-1}.

scales 5 Mpc$^{-1} \lesssim k \lesssim 40$ Mpc^{-1} (as large values of the power-spectrum slope $n_{\rm cut}$ are excluded). We show the 1σ and 2σ excluded values of $k_{\rm cut}$ and $n_{\rm cut}$, allowing other parameters to vary freely. We find a slight $\sim 1\sigma$ preference for enhanced power, which is due to the slight "turn up" of velocity dispersions at low $R_{\rm eff}$ in Fig. 4. This effect, however, is not statistically significant.

The results are intuitive: from Fig. 4, data approximately follow the CDM correlation between $\sigma^*_{\rm los}$ and $R_{\rm eff}$, with no clear sign of a break characteristic of LDM. This favors similar concentrations for all Milky Way satellites, i.e., similar formation times. As explained in Sec. II B, this favors close-to-scale-invariant power spectra.

Our analysis loses sensitivity for $k_{\rm cut} \lesssim 5$ Mpc^{-1} and $k_{\rm cut} \gtrsim 40$ Mpc^{-1}. This is intuitive; using Eq. (3), smaller k correspond to halo masses $M_{200c} \gtrsim 10^{11} M_\odot$, above the mass of a Milky Way satellite galaxy. Larger k correspond to halo masses $M_{200c} \lesssim 10^8 M_\odot$. The dwarfs with lowest half-light radii that we consider (Segue-I, Segue-II, and Willman-I) have $M_* \simeq 2 - 5 \times 10^2 M_\odot$, i.e., halo masses in that ballpark (see Fig. 5).

Our determination of the power spectrum is robust against baryonic effects and different galaxy-halo

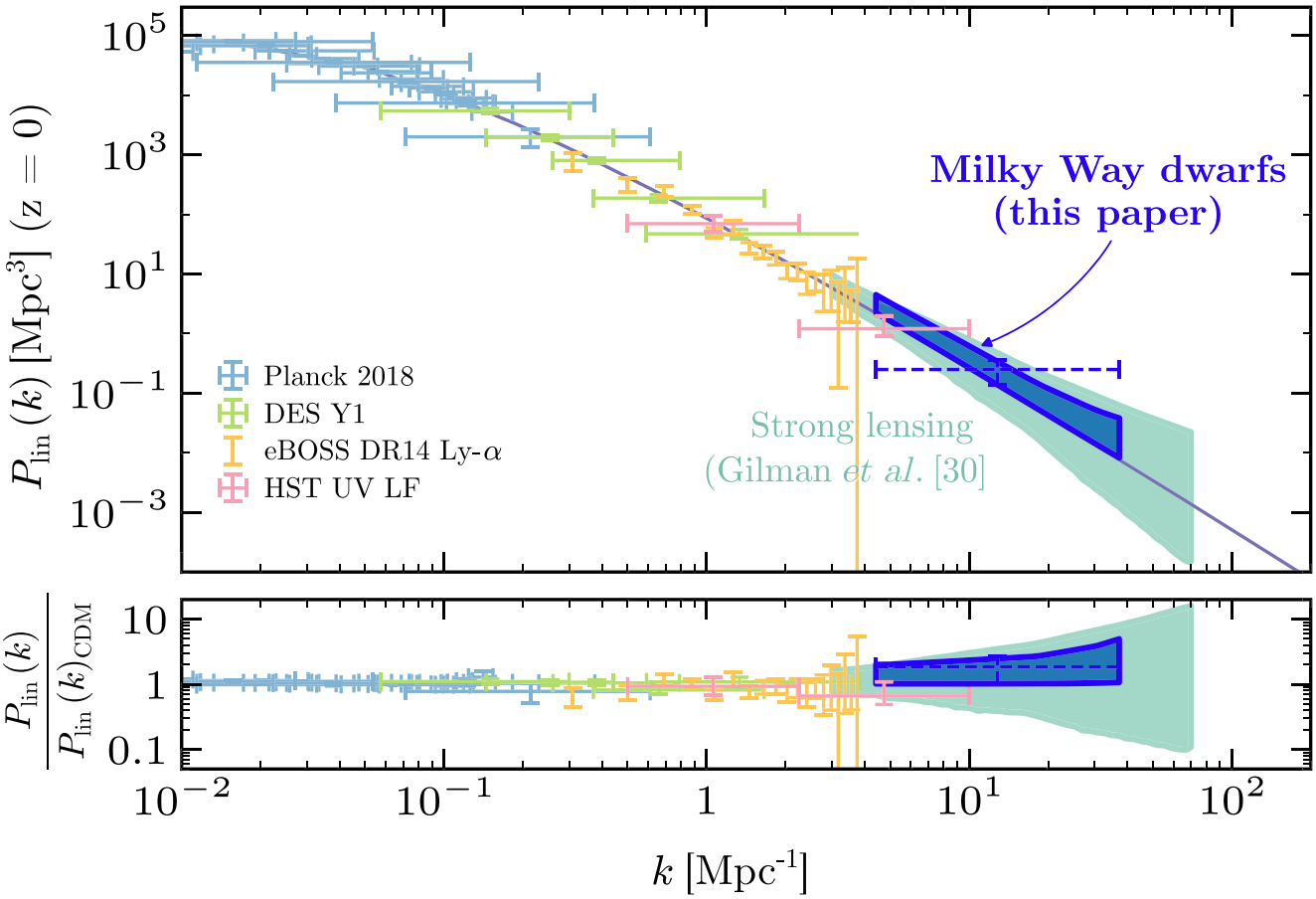

FIG. 8. 1σ allowed linear matter power spectrum in our analysis (shaded), its geometric mean (dashed), and previous data [3,30,32,157–159]. Dwarf galaxy velocity dispersion and size data is a unique, sharp probe of small-scale dark matter properties.

connection models. The strongest degeneracy we find is with the halo mass above which baryonic feedback makes DM density profiles cored, $M_{\rm thres}^{\rm core}$. By making low-mass halos cored, their velocity dispersion gets reduced, and LDM predictions resemble more those of CDM. However, a CDM-like correlation between $\sigma_{\rm los}^{*}$ and $R_{\rm eff}$ (see Fig. 4) is never fully mimicked. Data can tell apart LDM and CDM even if LDM halos are cored at all halo masses.

Figure 8 shows that dwarf galaxy velocities and sizes determine the DM power spectrum at small scales with unprecedented precision. We show existing measurements from Planck [157], DES [158], eBOSS Lyman-α [3,159], the UV luminosity function as measured by the Hubble Space Telescope [32], and strong gravitational lensing [30]; the first three measurements have been obtained using the `mpk_compilation` code [159,160]. Since our parametrization in Eq. (1) only allows for enhanced power spectra, for consistency we have ensured that the analysis does not prefer suppressed power spectra. To do so, we parametrize suppressed power with $n_{\rm cut} < n_s$ as $\mathcal{P}_{\mathcal{R}}(k) \propto k^{n_s-1}/[1+(k/k_{\rm cut})^{n_s-n_{\rm cut}}]$ and repeat our analysis extending the range to $n_{\rm cut} < 1$. That expression smoothly interpolates from $\mathcal{P}_{\mathcal{R}} \propto k^{n_s-1}$ at $k \ll k_{\rm cut}$ to $\mathcal{P}_{\mathcal{R}} \propto k^{n_{\rm cut}-1}$ at $k \gg k_{\rm cut}$. To aid the connection with $k_{\rm cut}$, we use units of Mpc^{-1} instead of $h\mathrm{Mpc}^{-1}$.

The dark shaded area in Fig. 8 encloses all power spectra in our 1σ allowed region for $\{k_{\rm cut}, n_{\rm cut}\}$, and the dashed data point is its geometric mean. Quantitatively,

$$\frac{P_{\rm lin}}{P_{\rm lin}^{\rm CDM}} = 1.81 \pm 0.80, \tag{18}$$

for $4\ \mathrm{Mpc}^{-1} < k < 37\ \mathrm{Mpc}^{-1}$. The range in k is where our analysis provides significant constraints. For other values of k, our uncertainties increase rapidly.

Our results are somewhat stronger than, and complementary to, the strong lensing determination in Ref. [30], which has different model assumptions and uncertainties.

Overall, our results add a high-precision, small-scale handle to the global picture of the primordial DM power spectrum being almost scale invariant across six orders of magnitude in wavenumber. We do so by exploiting sizes and kinematics of one of the smallest DM-dominated class of systems we know of: Milky Way satellite galaxies.

V. CONCLUSIONS AND FUTURE DIRECTIONS

The properties of DM at small scales remain uncertain. In this paper, we have shown that the correlation between dwarf galaxy internal velocities and sizes is a powerful probe to explore them. Our constraining power mostly comes from probing the concentration-mass relation of DM halos, in contrast to previous work focusing on halo abundances [13–20].

We focus on models that enhance the primordial matter power spectrum at small scales, that we denote as "Lumpy Dark Matter." This prediction is natural if DM is produced out of quantum fluctuations during inflation, which does not require nongravitational interactions with baryons [25–27]. We utilize semianalytic techniques and scaling relations, inspired by physics models and calibrated against simulations, to compute DM halo properties. We are agnostic about many aspects of the galaxy-halo connection, allowing us to marginalize over poorly understood baryonic effects, and carry out a joint analysis of internal velocities, sizes, and total abundance of classical and SDSS Milky Way satellites.

Regardless of the DM power spectrum, we constrain the stellar mass-halo mass relation, the halo occupation fraction, and tidal subhalo disruption. We find that halos with masses of $10^8 M_\odot$ and $10^9 M_\odot$ must host galaxies with stellar masses below $10^4 M_\odot$ and $10^6 M_\odot$, respectively; and our analysis disfavors strong tidal disruption. This is mostly inferred from the total satellite abundance, implying *little correlation with our determination of DM properties* that relies mostly on the correlation between stellar velocity dispersion and half-light radius.

We obtain a leading-precision determination of the DM power spectrum on subgalactic scales $4\ \mathrm{Mpc}^{-1} < k < 37\ \mathrm{Mpc}^{-1}$. Milky Way satellite properties imply that, at those scales, the DM power spectrum cannot deviate from scale invariance by more than a factor $\sim$2.5 at 1σ.

Our methodology can be easily extended in further work. On the DM side, many scenarios that modify the small-scale DM properties have been explored in the literature. Examples include Self-Interacting Dark Matter (SIDM) [8], Warm Dark Matter (WDM) [9,10], Fuzzy Dark Matter (FDM) [11], or a modified cosmological history [161,162]. They are theoretically and observationally motivated, and in many of them the power spectrum at small scales is suppressed. Their consequences for the correlation between velocity dispersions and half-light radii are unexplored. The fact that our analysis finds a slight preference for enhanced power spectra forecasts increased sensitivity to such models.

On the modeling side, in this paper we have been agnostic about the galaxy-halo connection. However, there are physically motivated models that predict the stellar mass-halo mass relation and the halo occupation fraction, as a function of halo concentration and assembly history [144,163–165]. Adding that information would improve the sensitivity to DM properties. For instance, higher concentration and earlier halo formation in LDM models may increase the stellar mass and the probability to host a galaxy [48] (as halos would be more massive before reionization and may form stars more efficiently), contradicting observations. Our data analysis methodology can also be used to test galaxy formation models. As mentioned in the Introduction, future work can also improve on the results presented here by running LDM simulations of halo and galaxy formation and evolution that could be tailored to

the Milky Way assembly history and include the associated uncertainties.

On the observational side, there is plenty of room for increased precision. We have only included classical and SDSS satellites (whose observations could be improved [136]), but our analysis can be extended to include Milky Way satellites discovered by the Dark Energy Survey, for which we are starting to get kinematic data (see, e.g., Refs. [74–78]) and whose completeness correction is understood [166]; Milky Way satellites discovered by DELVE [79–83]; M31 satellites, to avoid the possibility of the Milky Way being an outlier; or even field dwarfs, unaffected by host galaxy effects but whose completeness correction and DM-driven velocity dispersion is harder to model. In the future, the Rubin Observatory should discover many dwarfs, within and outside the Milky Way, and inform on their spatial distribution [167,168]. This would also quantify the amount of tidal disruption, which may be suppressed in LDM models as discussed above.

The satellite luminosity function can also be added to our dataset. This would better constrain the stellar mass-halo mass relation and the halo occupation fraction. Abundances, luminosities, sizes, and kinematics are the galaxy observables that most directly relate to DM halo features. Analyzing them together would provide a more complete picture of DM properties.

Finally, LDM models have a rich phenomenology that can be explored with other observables. As Fig. 2 shows, enhanced power spectra dramatically increase the formation redshift of low-mass halos, by breaking a fortuitous cancellation in the density variance of scale-invariant power spectra. This may produce stars early [48] and affect reionization, which can be explored with Cosmic Microwave Background [1,169,170] and 21 cm observations [171]. James Webb Space Telescope (JWST) observations are also providing a unique window to the high-redshift Universe and the formation of the first galaxies [172–184]. Precisely determining the UV luminosity function can be a sharp probe of the DM power spectrum, as shown by existing work with Hubble Space Telescope (HST) data [32,185] and first JWST results [49,186,187].

Evidence for an unknown dark matter, five times more abundant than regular matter, first appeared in galaxy observations [188,189]. This was confirmed to high accuracy observing the largest scales of our Universe [1,190]. By studying back small-scale dark matter-dominated systems with increased precision, we are now on our way to building a coherent picture of the properties of the second most abundant component of the Universe.

ACKNOWLEDGMENTS

We thank Andrew Benson for helpful comments, a careful reading of the manuscript, and collaboration in early stages of the project. We are grateful for helpful comments from John Beacom, Hector Cruz, Nicole Gountains, Zavier Kamath, and especially Xiaolong Du, Daniel Gillman, Jordi Miralda-Escude, Ethan Nadler, Nashwan Sabti, Chun-Hao To, and Katy Rodriguez Wimberly. A. H. G. P.'s work is supported in part by NSF Grant No. AST-2008110 and the NASA Astrophysics Theory Program, under Grant No. 80NSSC18K1014. I. E. acknowledges support from Basque Government (IT1628-22); Grant No. PID2021-123703NB-C21 funded by MCIN/AEI/10.13039/501100011033/ and by ERDF "A way of making Europe"; and Grant No. PID2022-136510NB-C33 funded by MCIN/AEI. Part of this work used the Solaris cluster, acquired through the Basque Government Grant No. IT1628-22.

APPENDIX A: IMPACT OF TIDAL STRIPPING, SUBHALO INFALL TIMES, THE VELOCITY ESTIMATOR, AND BARYONIC FEEDBACK

In this appendix, we quantify the approximations described in the main text. We show that including tidal stripping, the different subhalo infall times, a different $\sigma^*_{\rm los}$ estimator, or a different DM halo profile affects our observables less than the observational uncertainties and than the parameters that we set free—baryonic feedback that turns cusps into cores, the stellar mass-halo mass relation, the halo occupation fraction, and subhalo tidal disruption. If constraints on the latter are improved in future work and they stop dominating the error budget, these approximations may need revisiting.

1. Tidal stripping

In the main text, we neglect tidal stripping of subhalos by the Milky Way.

Figure 9 shows that tidal effects have a subleading impact on our observables. Both panels show the correlation between $\sigma^*_{\rm los}$ and $R_{\rm eff}$, together with data from classical and SDSS satellites, for the same halo-galaxy connection model and LDM parameters as Fig. 4, but including tidal effects in the dashed regions. In the left panel, we truncate the halo density profile beyond the tidal radius [30,91,125], as computed with `Galacticus` following Ref. [191] (we use the orbiting subhalo model, that follows subhalo positions and allows computing the tidal radius). In the right panel, we include tidal shocking and heating effects by changing halo structural parameters following the "tidal tracks" in Ref. [132]. We show only the CDM scenario to which Ref. [132] was calibrated. As mentioned in the main text, high concentrations of LDM halos may make them more resilient to tidal stripping [129,141], so similar or smaller effects are expected for LDM.

We observe that DM mass removal beyond the tidal radius has a negligible impact on our observables given the

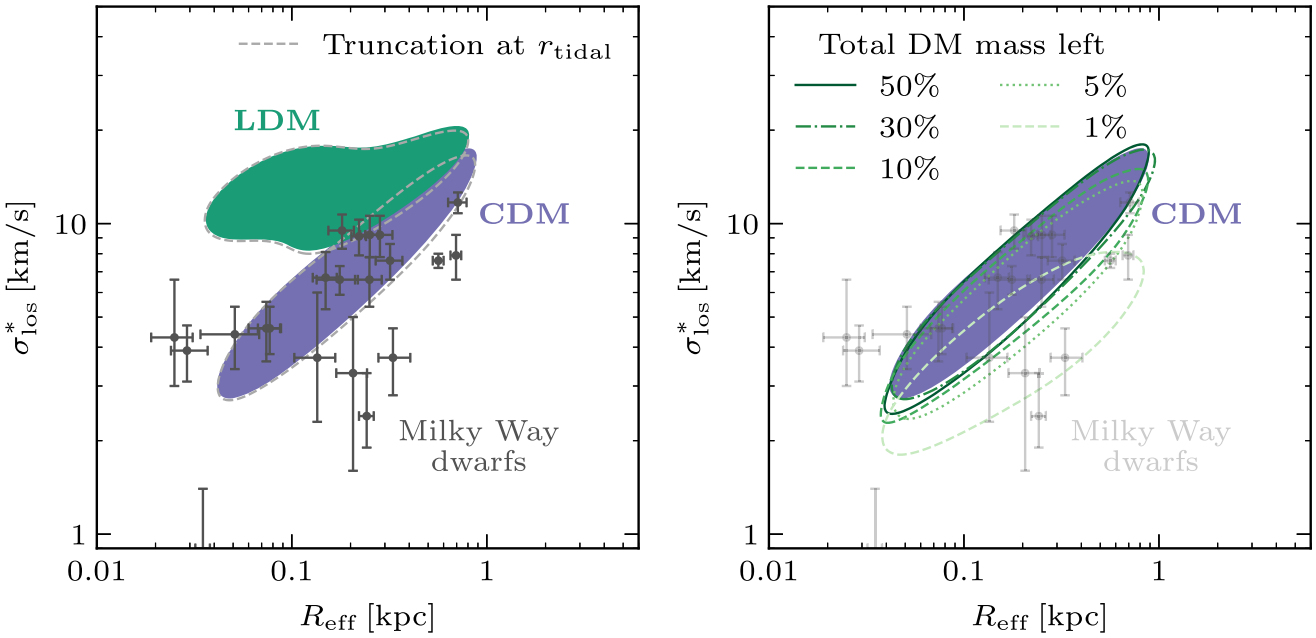

FIG. 9. Same as Fig. 4, but the dashed lines include tidal effects. To avoid crowding the figure, colored regions show 68% of the enclosed population. In the left panel, we truncate DM density profiles at the tidal radius. In the right panel, we include tidal shocking and heating by changing the halo structural parameters, following the "tidal tracks" in Ref. [132]. Tidal effects would have a subleading impact on our error budget.

precision of the data (see Fig. 13 below for the impact of the parameters that we set free). Tidal shocking and heating could have a significant impact, but this would require a large fraction of the DM halo population to lose more than 95%–99% of their mass. Simulations [135,137] and observations [136] disfavor such dramatic effects. Similar conclusions were reached in previous population studies: dwarf galaxies are located well inside their host DM halos, so very strong tidal stripping at the population level is needed to affect the conclusions [22,139,140].

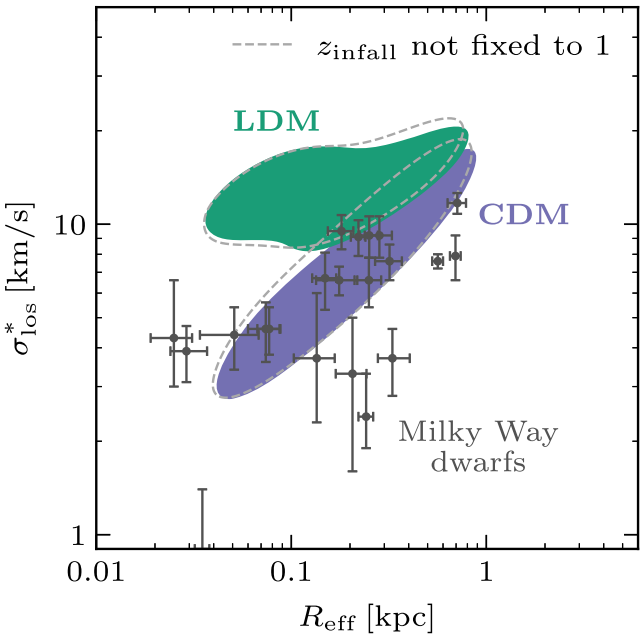

FIG. 10. Same as Fig. 4, but the dashed lines include the different satellite infall times. To avoid crowding the figure, colored regions show 68% of the enclosed population. Different infall times would have a subleading impact on our error budget.

2. Infall times

In the main text, we evaluate all Milky Way satellite properties at median infall redshift $z_{\rm infall} = 1$ [37–39].

Figure 10 shows that including the different infall redshifts has a subleading impact on our observables. We show the correlation between $\sigma^*_{\rm los}$ and $R_{\rm eff}$, together with data from classical and SDSS satellites, for the same halo-galaxy connection model and LDM parameters as Fig. 4, but evaluating halo properties at infall redshift as computed with `Galacticus` in dashed.

We observe that the impact on our observables is negligible given the precision of the data (see Fig. 13 below for the impact of the parameters that we set free). The main effect is to slightly increase $\sigma^*_{\rm los}$. This is because the $z_{\rm infall}$ distribution is skewed towards $z_{\rm infall} > 1$ [37–39], and internal halo velocities are higher at high redshift [22].

3. Velocity estimator

In the main text, we estimate $\sigma^*_{\rm los}$ using Eq. (12) that was obtained in Ref. [111]. This was shown to be robust against stellar velocity dispersion anisotropy. Reference [192]

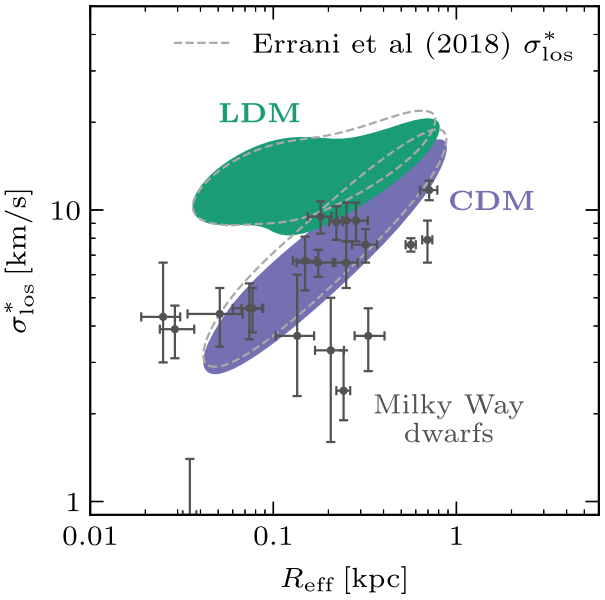

FIG. 11. Same as Fig. 4, but the dashed lines use the $\sigma^*_{\rm los}$ estimator from Ref. [192]. To avoid crowding the figure, colored regions show 68% of the enclosed population. A recent mass estimator would have a subleading impact on our error budget.

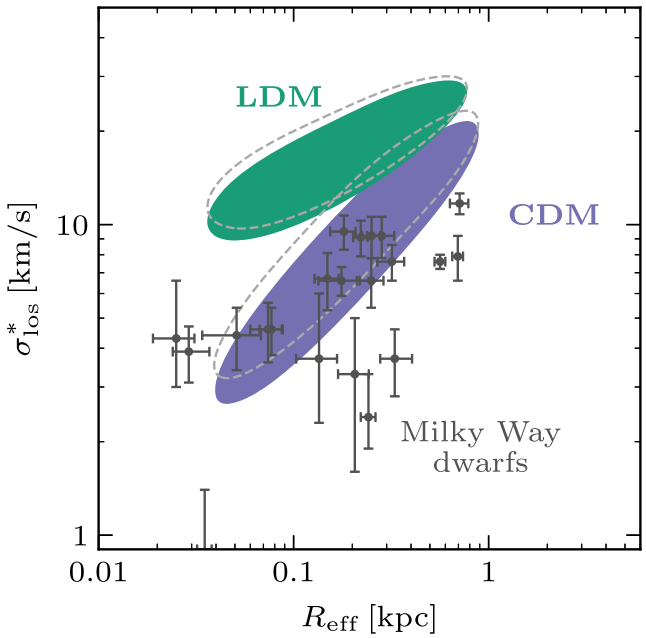

FIG. 12. Same as Fig. 4, but the dashed lines assume an Einasto profile and the solid region an NFW profile. To avoid crowding the figure, colored regions show 68% of the enclosed population. Assuming an Einasto profile would have a subleading impact on our error budget.

proposed a different estimator, also robust against the shape of the inner halo profile and how deeply the stellar component is embedded within the halo. By comparing with simulation, the latter estimator was shown to have an accuracy of ∼10% (better than our observational uncertainties).

Figure 11 shows that using the estimator from Ref. [192] has a subleading impact on our observables. We show the correlation between $\sigma^*_{\rm los}$ and $R_{\rm eff}$, together with data from classical and SDSS satellites, for the same halo-galaxy connection model and LDM parameters as Fig. 4, but with the estimator from Ref. [192] in the dashed regions.

We observe that the impact on our observables is negligible given the precision of the data (see Fig. 13 below for the impact of the parameters that we set free).

4. DM halo profile

In the main text, we assume that, before baryonic feedback induces cores, DM halo profiles follow an NFW form, Eq. (6).

Figure 12 shows that assuming an Einasto form [193]

$$\rho(r) = \rho_s e^{-\frac{2}{\alpha}[(r/r_s)^\alpha - 1]} \tag{A1}$$

has a subleading impact on our observables. We show the correlation between $\sigma^*_{\rm los}$ and $R_{\rm eff}$, together with data from classical and SDSS satellites. We use the same halo-galaxy connection model and LDM parameters as Fig. 4, but assuming an Einasto profile in dashed and, for consistency, a cuspy NFW profile at all halo masses in solid. For the Einasto profile, we set $\alpha = 0.16$, which was found in Ref. [63] to be a good fit for a very wide range in halo masses.

We observe that the impact on our observables is negligible given the precision of the data (see Fig. 13 below for the impact of the parameters that we set free).

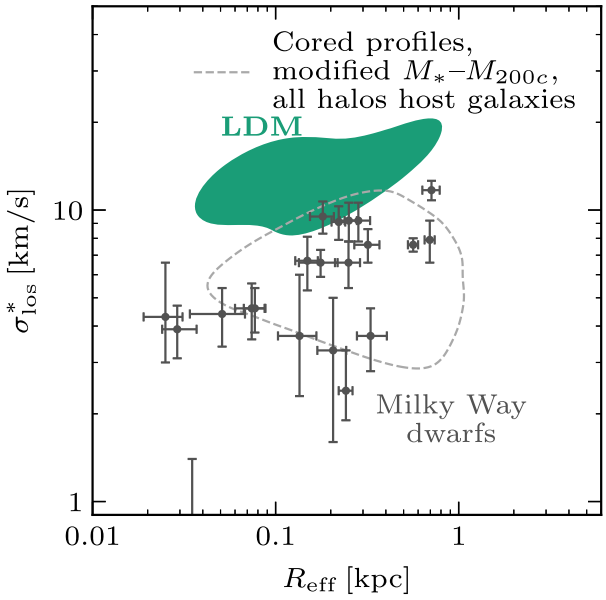

FIG. 13. Same as Fig. 4, but for the dashed line we change our free parameters. To avoid crowding the figure, colored regions show 68% of the enclosed population for the LDM case. Our error budget is dominated by the parameters we set free.

The main effect is to slightly increase $\sigma^*_{\rm los}$. This is because for radii $\gtrsim 10^{-3} r_s$ an Einasto profile encloses more mass than an NFW profile with the same mass and concentration, and the half-light radii we consider are larger than $10^{-3} r_s$.

5. Baryonic feedback

Here, we illustrate the effects of some parameters that we set free in our analysis: baryonic feedback that turns NFW "cusps" into "cores," the uncertain stellar mass-halo mass relation, and the uncertain halo occupation fraction. As discussed in the main text, the first effect is the most degenerate with our determination of the power spectrum.

Figure 13 shows that the parameters that we set free in our analysis significantly affect our observables. We show the correlation between $\sigma^*_{\rm los}$ and $R_{\rm eff}$, together with data from classical and SDSS satellites, for the same halo-galaxy connection model and LDM parameters as Fig. 4, but changing our free parameters in the dashed region. To generate the dashed region we set cored profiles for all halo masses, we change the scatter of the stellar mass-halo mass relation by setting $\sigma^{M_*} = 0.8$ and $\gamma^{M_*} = -0.6$, and we set the halo occupation fraction to 1 at all halo masses. Importantly, these parameters are allowed by our analysis. Other parameters are set as in Fig. 4.

We observe that, even if changing our free parameters has a strong impact, the LDM correlation between $\sigma^*_{\rm los}$ and $R_{\rm eff}$ is still different from CDM. For this correlation to be affected by baryons, *baryonic feedback would have to induce increasingly strong cores at lower halo masses*, compensating the enhanced LDM mass-concentration relation in Fig. 2. This would be opposite to conventional wisdom, simulation, and observations—lower mass halos tend to be increasingly "cuspy" as they have too few stars to instigate core formation [120,121,124].

APPENDIX B: STATISTICAL ANALYSIS

We obtain the quantitative conclusions in the main text through a statistical analysis of Milky Way satellite properties. In this appendix, we describe in detail this analysis.

We fit for the half-light radius, stellar velocity dispersion, and total number of classical and SDSS Milky Way satellites, using the data collected in Refs. [22,100,156] and updated as of 2021 in this Ref. [194]. For reference, we compile the numerical values in Appendix D. We do not include the Magellanic clouds, Pisces II, and Sagittarius, as baryonic effects and strong tidal stripping could bias our results (the impact of this is minor, as they are a small fraction of our sample). We carry out a frequentist unbinned maximum likelihood (also called profile likelihood in the literature),

$$-2\ln\mathcal{L} = -2\sum_i \ln\mu(\sigma^{*{\rm obs},i}_{\rm los}, R^{{\rm obs},i}_{\rm eff}) - 2\ln\mathcal{P}(N_{\rm obs}). \quad \text{(B1)}$$

$\mu(\sigma^{*\rm obs}_{\rm los}, R^{\rm obs}_{\rm eff})\mathrm{d}\sigma^{*\rm obs}_{\rm los}\mathrm{d}R^{\rm obs}_{\rm eff}$ is the differential probability for a satellite galaxy to have an *observed* stellar velocity dispersion $\sigma^{*\rm obs}_{\rm los}$ and half-light radius $R^{\rm obs}_{\rm eff}$. $\sigma^{*{\rm obs},i}_{\rm los}$ and $R^{{\rm obs},i}_{\rm eff}$ are the observed stellar velocity dispersions and half-light radii, respectively. $\mathcal{P}(N_{\rm obs})$ is the probability to observe $N_{\rm obs}$ satellite galaxies, with $N_{\rm obs} = 21$ the number of observed satellites. The first probability is given by

$$\mu(\sigma^{*\rm obs}_{\rm los}, R^{\rm obs}_{\rm eff}) = \int \mathcal{P}(\sigma^*_{\rm los}, R_{\rm eff}, c, M_*, M)\frac{1}{\sqrt{2\pi}\Delta\sigma} e^{-\frac{(\sigma^{*\rm obs}_{\rm los}-\sigma^*_{\rm los})^2}{2\Delta\sigma^2}} \times \frac{1}{\sqrt{2\pi}\Delta R_{\rm eff}} e^{-\frac{(R^{\rm obs}_{\rm eff}-R_{\rm eff})^2}{2\Delta R^2_{\rm eff}}} \mathrm{d}\sigma^*_{\rm los}\mathrm{d}R_{\rm eff}\mathrm{d}c\mathrm{d}M_*\mathrm{d}M. \quad \text{(B2)}$$

$\mathcal{P}(\sigma^*_{\rm los}, R_{\rm eff}, c, M_*, M)\mathrm{d}\sigma^*_{\rm los}\mathrm{d}R_{\rm eff}\mathrm{d}c\mathrm{d}M_*\mathrm{d}M$ is the differential probability to observe a galaxy with *true* velocity dispersion $\sigma^*_{\rm los}$, half-light radius $R_{\rm eff}$, concentration c, stellar mass M_*, and DM halo mass M (for simplicity, in this appendix we denote $M_{200c} \equiv M$). The two Gaussians are the probabilities to observe a velocity dispersion $\sigma^{*\rm obs}_{\rm los}$ and half-light radius $R^{\rm obs}_{\rm eff}$, given their true values $\sigma^*_{\rm los}$ and $R_{\rm eff}$ respectively, with $\Delta\sigma$ and $\Delta R_{\rm eff}$ the observational uncertainties. We assume Gaussian uncertainties for simplicity, as our quantitative statements are only 1σ–2σ away from the best fit. We conservatively ignore correlations among $\Delta\sigma$ and $\Delta R_{\rm eff}$. Should correlations or non-Gaussian uncertainties be provided by observations, they would be straightforward to include. We consider halo masses between $10^7 M_\odot$ and $10^{12} M_\odot$. Lower-mass halos would be too dim to be observed, as we discuss in Sec. IV A (see also Ref. [17]); and higher-mass halos would be heavier than the Milky Way.

The expression can be further simplified using conditional probabilities,

$$\begin{aligned}\mathcal{P}(\sigma^*_{\rm los}, R_{\rm eff}, c, M_*, M) &= \mathcal{P}(\sigma^*_{\rm los}, R_{\rm eff}, c, M_*|M)\mathcal{P}(M)\\ &= \mathcal{P}(\sigma^*_{\rm los}, R_{\rm eff}|c, M_*, M)\mathcal{P}(c, M_*|M)\mathcal{P}(M)\\ &= \mathcal{P}(\sigma^*_{\rm los}|R_{\rm eff}, c, M_*, M)\mathcal{P}(R_{\rm eff}|c, M_*, M)\mathcal{P}(c, M_*|M)\mathcal{P}(M), \end{aligned} \quad \text{(B3)}$$

where

(1) $\mathcal{P}(M)$ is the product of the subhalo mass function at infall redshift (see Sec. I in the main text) and the halo occupation fraction. We compute the former with `Galacticus` following Refs. [46,52,53,56] as described in the main text (Sec. II A), and we parametrize the latter as described in the main text [Eq. (13), Sec. III A]

$$\mathrm{hof}(M) = \frac{1 + \mathrm{erf}(\alpha^{\mathrm{hof}} \log_{10}[M/M_0^{\mathrm{hof}}])}{2}, \quad \text{(B4)}$$

with erf the error function, and $\alpha^{\mathrm{hof}} > 1$ [35,71] and M_0^{hof} free parameters. M is the infall mass [145].

(2) Following the observational results in Ref. [22], we assume that R_{eff} only depends on stellar mass, i.e., $\mathcal{P}(R_{\mathrm{eff}}|c, M_*, M) = \mathcal{P}(R_{\mathrm{eff}}|M_*)$. As described in the main text [Eq. (9), Sec. III A], we assume a lognormal distribution with median $\overline{R_{\mathrm{eff}}} = 7.76 \times 10^{-3} M_*^{0.268}$ and scatter of 0.234 dex [22].

As R_{eff} only links to halo mass via the stellar mass-halo mass relation, that we set free (see below), observational uncertainties on $\mathcal{P}(R_{\mathrm{eff}}|M_*)$ do not have a strong impact on our error budget. We also set free the halo occupation fraction, which makes the connection between DM halos and M_* even more flexible.

(3) We assume that c and M_* are independent and only related to M, $\mathcal{P}(c, M_*|M) = \mathcal{P}(c|M)\,\mathcal{P}(M_*|M)$. Then,

(i) $\mathcal{P}(c|M)$ is, as described in the main text (Sec. II A), a lognormal distribution with median computed with `Galacticus` following Ref. [62] and scatter of 0.16 dex [64].

(ii) $\mathcal{P}(M_*|M)$ is the product of the probability to observe the galaxy given its stellar mass, parametrized by the completeness correction; and the stellar mass-halo mass relation.

For the completeness correction, we follow Eqs. (14) and (15) in the main text (Sec. III A). As explained in the main text, the completeness correction takes into account the dependence both on M_* and R_{eff} [148].

In principle, the completeness correction could be affected by low-surface-brightness uncertainties in the M_*–R_{eff} relation due to low selection efficiency. These have a minor impact on the *shape* of the distribution of galaxies, i.e., $\mu(\sigma_{\mathrm{los}}^{*\mathrm{obs}}, R_{\mathrm{eff}}^{\mathrm{obs}})$; because they affect galaxies with a very low observation probability that are not included in our analysis (see, e.g., Fig. 4 in Ref. [195]): we conservatively only include galaxies with an observation probability larger than 90% (although the transition is rather sharp, see Ref. [148]). In turn, the *total number* of galaxies, i.e., $\mathcal{P}(N_{\mathrm{obs}})$; could be affected more significantly. However, we have checked that low-surface-brightness uncertainties do not change the number of expected galaxies by more than 10% (see also, e.g., Fig. 12 in Ref. [73]), which is a subdominant contribution to our error budget (see below).

We include anisotropy-induced scatter as described in the main text (Sec. IV): we multiply $\mathcal{C}_\Omega$ by a free parameter $\sigma_{\mathcal{C}_\Omega}$, and we add to the likelihood a Gaussian prior on $\sigma_{\mathcal{C}_\Omega}$ centered at 1 and with 19% width [13] (this is a conservative estimate, derived when SDSS was not yet complete). We also include uncertainty in the spatial satellite distribution $n(r)$ due to tidal disruption, by parametrizing $n(r)$ as described in the main text [Eq. (17), Sec. IV]

$$n(r) = n_{\mathrm{GK17}}(r) + y_{\mathcal{C}}[n_{\mathrm{NFW}}(r) - n_{\mathrm{GK17}}(r)], \quad \text{(B5)}$$

with $y_{\mathcal{C}} \in [0, 1]$ a free parameter that interpolates between an NFW distribution, $n_{\mathrm{NFW}}(r)$, and the tidally disrupted distribution from Ref. [149], $n_{\mathrm{GK17}}(r)$. The latter distribution strongly suppresses the subhalo abundance within the inner ∼100 kpc. Enhancements in the number of subhalos within the inner ∼50 kpc due to the recent passage of the Large Magellanic Cloud [68–70] are smaller than the tidal disruption uncertainty we parametrize by $y_{\mathcal{C}}$.

For the stellar mass-halo mass relation, we follow Eqs. (10) and (11) in the main text (Sec. III A). I.e., we assume it to be a lognormal distribution whose median follows a power law with power β^{M_*} and normalization $M_*(M = 1.54 \times 10^{12} M_\odot) = 0.0455M$ [104], and whose scatter can increase at low mass, [108]

$$\sigma(M) = \sigma^{M_*} + \gamma^{M_*} \log_{10} \frac{M}{10^{11} M_\odot} \mathrm{dex}. \quad \text{(B6)}$$

β^{M_*}, $\sigma^{M_*} \in [0, 2]$ [71,108], and $\gamma^{M_*} < 0$ are free parameters. M is the infall mass [104].

(4) $\mathcal{P}(\sigma_{\mathrm{los}}^*|R_{\mathrm{eff}}, c, M_*, M) = \delta(\sigma_{\mathrm{los}}^* - \sqrt{\frac{G}{4} \frac{M(<R_{\mathrm{eff}}/0.75)}{R_{\mathrm{eff}}}})$ [Eq. (12) and Sec. III A in the main text], which depends on M and c through the enclosed mass $M(< r)$. For simplicity we ignore scatter, as other mass estimators produce very similar results [16] (see also Fig. 11). As described in the main text (Secs. II A and III A), we include baryonic feedback by assuming an NFW profile for $M < M_{\mathrm{thres}}^{\mathrm{core}}$ and a cored profile for $M > M_{\mathrm{thres}}^{\mathrm{core}}$ following Ref. [124] (where the core size depends on the time over which a galaxy has formed stars), with $M_{\mathrm{thres}}^{\mathrm{core}}$ a free parameter.

Since μ is a differential probability, we numerically normalize it so that $\int \mu(\sigma_{\rm los}^{*\rm obs}, R_{\rm eff}^{\rm obs}) {\rm d}\sigma_{\rm los}^{*\rm obs} {\rm d}R_{\rm eff}^{\rm obs} = 1$.

Finally, for the probability to observe $N_{\rm obs}$ satellite galaxies $\mathcal{P}(N_{\rm obs})$ we follow Ref. [196] and include the additional scatter due to differences in the host halo's accretion histories [197] by modeling $\mathcal{P}(N_{\rm obs})$ with a negative binomial distribution with 18% intrinsic scatter and mean

$$N_{\rm expected} = \int \mathcal{P}(\sigma_{\rm los}^{*}, R_{\rm eff}, c, M_*, M) {\rm d}c {\rm d}M_* {\rm d}M {\rm d}\sigma_{\rm los}^{*} {\rm d}R_{\rm eff}, \tag{B7}$$

i.e., $\mathcal{P}(\sigma_{\rm los}^{*}, R_{\rm eff}, c, M_*, M)$ is normalized to the expected number of observed galaxies. This integral is dominated by low-mass halos (see Fig. 3), so the effect of not including the Magellanic clouds in our analysis is minor. However, the Large Magellanic Cloud accretes small-mass satellites with it, changing the expected number of satellites by up to tens of percent [68–73] (although we use satellites discovered by SDSS, whose footprint does not contain the Magellanic Clouds). On top of that, changing the Milky Way mass within uncertainties [40] would change $N_{\rm expected}$ by about 20% [22]. Both effects are smaller than the total scatter of $\mathcal{P}(N_{\rm obs})$. In addition, our main constraining power on DM properties does not come from the total number of satellites, as that is degenerate with galaxy-halo connection parameters (see Sec. IV A in the main text).

Overall, our likelihood $\mathcal{L}$ depends on 2 parameters describing DM physics, $\{n_{\rm cut}, k_{\rm cut}\}$; and 8 parameters modelling galaxy properties and baryonic effects, $\{M_0^{\rm hof}, \alpha^{\rm hof}, \beta^{M_*}, \sigma^{M_*}, \gamma^{M_*}, M_{\rm thres}^{\rm core}, \sigma_{\mathcal{C}_\Omega}, y_{\mathcal{C}}\}$. To obtain allowed regions in a subset of parameters, we minimize $-2\ln\mathcal{L}$ over other parameters. We draw contours corresponding to $\Delta 2\ln\mathcal{L} = 1.0$ and 4.0 for one-parameter scans; and to $\Delta 2\ln\mathcal{L} = 2.30$ and 6.18 for two-parameter scans. Under the assumption that Wilks' theorem [198] holds, these can be interpreted as 68% (1σ) and 95% (2σ) confidence level regions. We note that this theorem requires the true values to be well-contained within the parameter space range and a large sample size; and we use broad scan ranges (see Appendix C for a discussion and visualization of the results), plus the amount of data (21 values of $\sigma_{\rm los}^{*}$, 21 values of $R_{\rm eff}$, and the total number of galaxies) is relatively large. We carry out the integrals with the VEGAS package [199] and the minimizations with the Py-BOBYQA package [200,201].

APPENDIX C: FULL PARAMETER SPACE SCAN

In this appendix, we provide the full results of our statistical analysis.

Table I shows our free parameters, the ranges over which we scan in our analysis (in a Bayesian framework, these would correspond to the prior ranges), and the 1σ preferred ranges after minimizing $-2\ln\mathcal{L}$ over all other parameters. We find that we can constrain many galaxy-halo connection parameters, such as the slope of the stellar

TABLE I. Parameters in our analysis. The parameters whose 1σ range has a * are strongly correlated with other parameters (see Fig. 14); meaningful constraints can be derived when other parameters are fixed. For the theoretical population in Fig. 4, we use illustrative galaxy-halo connection parameters (see references). Some scan ranges are physics-motivated (see references).

	$k_{\rm cut}/{\rm Mpc}^{-1}$	$n_{\rm cut}$	$M_0^{\rm hof}/M_\odot$	$\alpha^{\rm hof}$	β^{M_*}
Meaning	Scale above which $P(k)$ is enhanced	Slope of the enhanced $P(k)$	Halo mass above which halos host galaxies	Steepness of the halo occupation fraction	Slope of the stellar mass-halo mass relation
Definition	Eq. (1)	Eq. (1)	Eq. (13)	Eq. (13)	Eq. (10)
Value in Fig. 4	8	2.6	$10^{8.35}$ [38,145]	1.31 [38,145]	0.963 [104]
Scan range	(4, 45)	(1, 5)	(10^7, 10^{11})	(1, 10) [35,71]	(0, 3)
1σ range	$(4, 45)^*$	$(1, 5)^*$	(10^7, $10^{7.9}$)	(1, 10)	(1.0, 1.7)

	σ^{M_*}/dex	γ^{M_*}/dex	$M_{\rm thres}^{\rm core}/M_\odot$	$y_{\mathcal{C}}$	$\sigma_{\mathcal{C}_\Omega}$
Meaning	Stellar mass-halo mass scatter at $10^{11}M_\odot$	Mass dependence of stellar mass-halo mass scatter	Halo mass below which DM profiles are cored	Amount of tidal halo disruption	Anisotropy in the satellite distribution
Definition	Eq. (11)	Eq. (11)	Below Eq. (12)	Eq. (17)	Below Eq. (17)
Value in Fig. 4	0.15 [104]	0 [104]	$10^9 M_\odot$ [22]	1	1
Scan range	(0, 2) [71,108]	$(-2, 0)$	(10^7, 10^{11})	(0, 1)	(0, 2)
1σ range	(0, 1.5)	$(-0.6, -0.2)$	(10^7, $10^{7.2}$)	(0.4, 1)	(0.87, 1.14)

mass-halo mass relation, the turning mass of the halo occupation fraction, the halo mass above which baryonic feedback makes DM density profile cored, or the amount of subhalo tidal disruption. Other parameters, such as the slope of the halo occupation fraction or the low-mass growth of stellar mass-halo mass scatter, are more challenging to constrain.

Figure 14 shows the correlations among our free parameters. To better visualize correlations between galaxy-halo connection parameters and enhanced power spectra (i.e., $n_{\rm cut} > 1$), we fix $k_{\rm cut} = 10\ {\rm Mpc}^{-1}$. Otherwise, for large enough $k_{\rm cut}$, any value of $n_{\rm cut}$ would be degenerate in our halo mass range with a scale-invariant power spectrum (see Figs. 2 and 7). We show the preferred 1σ and 2σ regions after minimizing $-2\ln\mathcal{L}$ over all other parameters. We find that, even though there are correlations among galaxy-halo connection parameters—particularly for the stellar mass-halo mass relation—, enhanced power, i.e., a modified $n_{\rm cut}$,

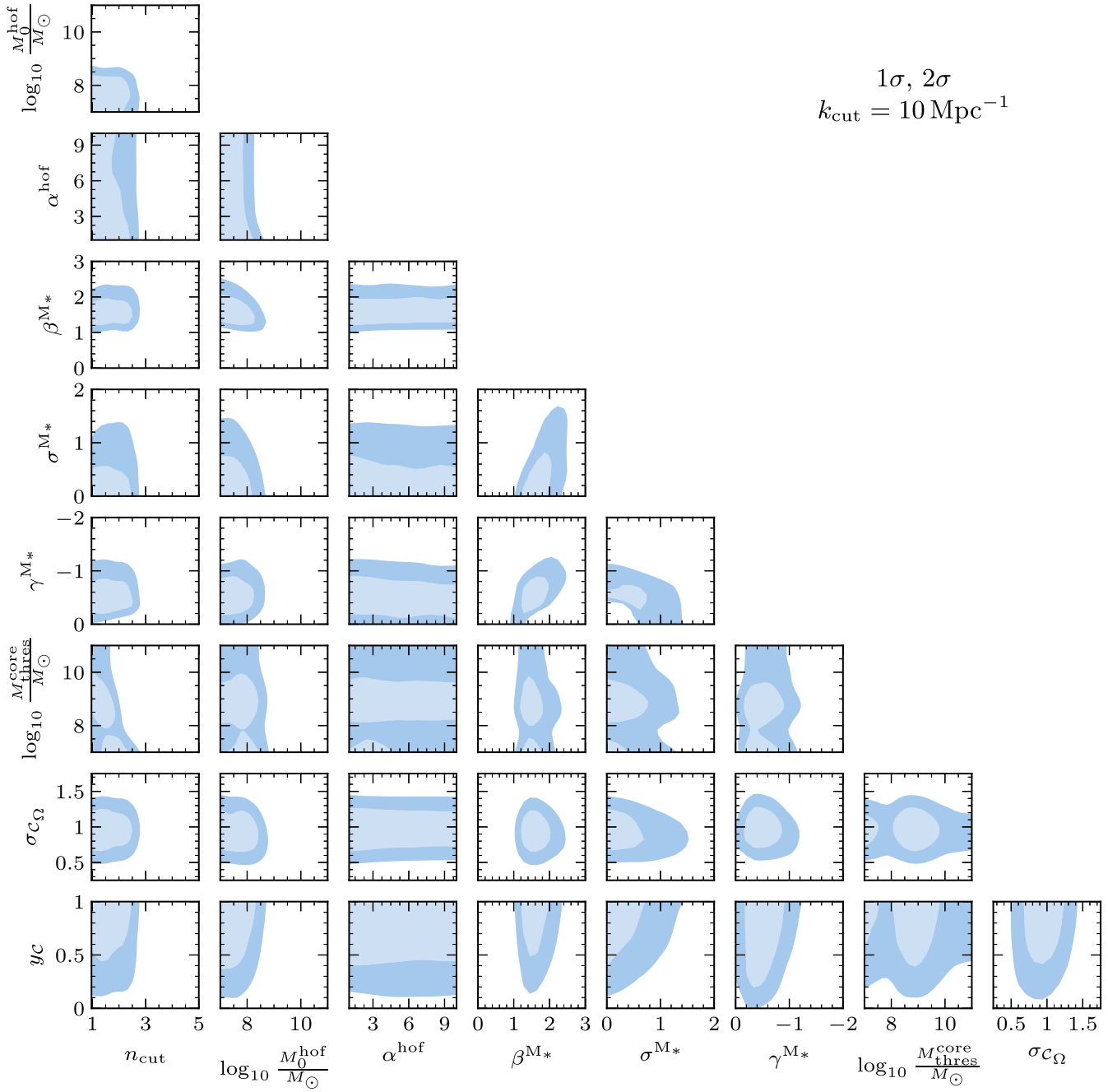

FIG. 14. Allowed regions within 1σ and 2σ for all parameters in our analysis. For each pair of parameters shown, all other parameters are minimized over in the likelihood. To visualize correlations with our determination of the power spectrum, we fix $k_{\rm cut} = 10\ {\rm Mpc}^{-1}$. Parameters controlling galaxy-halo connection and baryonic feedback are mostly independent of the DM power spectrum.

TABLE II. List of data used in the analysis.

Galaxy	$\sigma^*_{\rm los}$ [km/s]	$R_{\rm eff}$ [kpc]
Fornax	11.7 ± 0.9	0.710 ± 0.077
Leo I	9.2 ± 1.4	0.251 ± 0.027
Sculptor	9.2 ± 1.4	0.283 ± 0.045
Leo II	6.6 ± 0.7	0.176 ± 0.042
Sextans I	7.9 ± 1.3	0.695 ± 0.044
Carina	6.6 ± 1.2	0.250 ± 0.039
Draco	9.1 ± 1.2	0.221 ± 0.019
Ursa Minor	9.5 ± 1.2	0.181 ± 0.027
Canes Venatici I	7.6 ± 0.4	0.564 ± 0.036
Hercules	3.7 ± 0.9	$0.330^{+0.075}_{-0.052}$
Galaxy	$\sigma^*_{\rm los}$ [km/s]	$R_{\rm eff}$ [kpc]
Bootes I	$2.4^{+0.9}_{-0.5}$	0.242 ± 0.021
Leo IV	3.3 ± 1.7	0.206 ± 0.037
Ursa Major I	7.6 ± 1.0	0.319 ± 0.050
Leo V	$3.7^{+2.3}_{-1.4}$	0.135 ± 0.032
Canes Venatici II	4.6 ± 1.0	0.074 ± 0.014
Ursa Major II	6.7 ± 1.4	0.149 ± 0.021
Coma Berenices	4.6 ± 0.8	0.077 ± 0.010
Bootes II	4.4 ± 1.0	0.051 ± 0.017
Willman 1	$4.3^{+2.3}_{-1.3}$	0.025 ± 0.006
Segue II	< 1.4	0.035 ± 0.003
Segue I	3.9 ± 0.8	$0.029^{+0.008}_{-0.005}$

is mostly independent of galaxy-halo connection as described in the main text (Sec. IV A). As discussed in Sec. IV B, the main correlation of enhanced power is with the halo mass above which baryonic feedback makes DM density profiles cored, i.e., $M^{\rm core}_{\rm thres}$. This makes our main conclusions robust even though for some parameters the 1σ range is bounded by the scan range. In more detail, our analysis does not fully bound the following parameters,

(i) $M^{\rm hof}_0$ and $M^{\rm thres}_{\rm core}$: both the 1σ range and the scan range stop at $10^7 M_\odot$. As discussed in Appendix B, this corresponds to the smallest halo mass we consider in our analysis, so smaller values of $M^{\rm hof}_0$ and/or $M^{\rm thres}_{\rm core}$ would produce the same results.

(ii) $y_{\mathcal{C}}$: both the 1σ range and the scan range stop at 1. As discussed in Appendix B, $y_{\mathcal{C}} = 1$ corresponds to no tidal halo disruption, so this is a physical boundary.

(iii) $\alpha^{\rm hof}$: the 1σ range covers the whole scan range. From Eq. (13), large $\alpha^{\rm hof}$ makes the transition in the halo occupation fraction more steep. At $\alpha^{\rm hof} = 10$ the transition is already a step function for all purposes, so higher $\alpha^{\rm hof}$ would produce the same result. In turn, $\alpha^{\rm hof} < 1$ would make the halo occupation fraction so flat that very heavy ($M \gtrsim 10^{11} M_\odot$) dark halos would be predicted, against simulations (see, e.g., Ref. [35]) and observations.

(iv) σ^{M_*}: both the 1σ range and the scan range stop at 0. This corresponds to the physical boundary of scatter being positive.

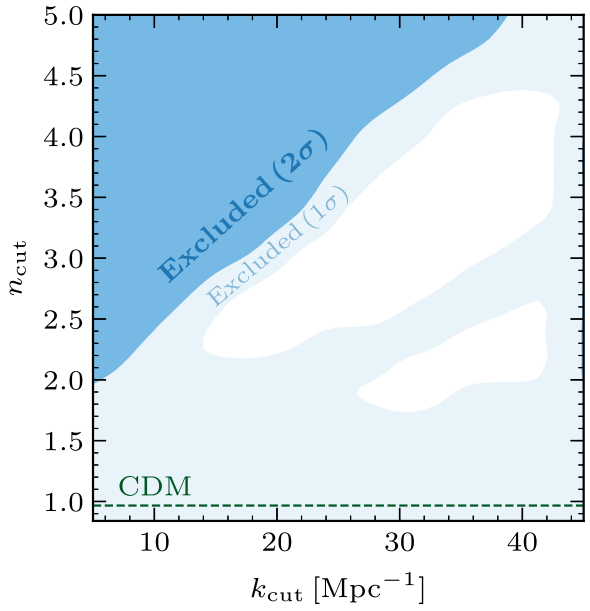

FIG. 15. Excluded values of LDM parameter space in our analysis, if the original determination of $\sigma^*_{\rm los}$ for Segue II is used.

APPENDIX D: DATA USED IN THE ANALYSIS

For reference, in this appendix we compile the data used in our analysis, see Table II, as obtained from Ref. [100]. As in Ref. [22], for Bootes II we adopt $\sigma^*_{\rm los} = 4.4 \pm 1$ km/s, instead of $\sigma^*_{\rm los} = 10.5 \pm 7.4$ km/s as listed in Ref. [100]. As discussed in Ref. [22], our value is based on a determination that employs more stars.

In addition, for Segue II the original determination quoted in Ref. [100], $\sigma^*_{\rm los} = 3.4^{+2.5}_{-1.2}$ km/s [202], was later reanalyzed, leading only to an upper limit $\sigma^*_{\rm los} < 1.4$ km/s (68% CL) [156]. Figure 15 shows the excluded values of LDM parameters if we carry out our analysis with the original determination. Comparing with Fig. 7, where Segue II is included as an upper limit, we see that the results are similar in both scenarios. Since the measurements leading to the upper limit contain a larger spectroscopic sample, and the resulting constraint on LDM models is more conservative; we have chosen $\sigma^*_{\rm los} < 1.4$ km/s for our main analysis. We note that, even though the low velocity dispersion of Segue II may be the outcome of significant tidal stripping, it is only a $\sim 2\sigma$ outlier from the overall trend in Fig. 4. Such outliers are to be expected given that we consider ~ 20 galaxies. Furthermore, the similar results obtained in our analysis with the original determination and with the upper limit emphasize that our population study is sensitive to *average* galaxy properties. Hence, it is reasonably robust against outliers.

We implement galaxies with asymmetric error bars in Eq. (B1) by using asymmetric split-Gaussian distributions.

[1] N. Aghanim *et al.* (Planck Collaboration), Planck 2018 results. VI. Cosmological parameters, Astron. Astrophys. **641**, A6 (2020); **652**, C4(E) (2021).

[2] T. M. C. Abbott *et al.* (DES Collaboration), Dark Energy Survey Year 3 results: Cosmological constraints from galaxy clustering and weak lensing, Phys. Rev. D **105**, 023520 (2022).

[3] M. R. Blanton *et al.* (SDSS Collaboration), Sloan Digital Sky Survey IV: Mapping the Milky Way, nearby galaxies and the distant universe, Astron. J. **154**, 28 (2017).

[4] J. S. Bullock and M. Boylan-Kolchin, Small-scale challenges to the ΛCDM paradigm, Annu. Rev. Astron. Astrophys. **55**, 343 (2017).

[5] M. R. Buckley and A. H. G. Peter, Gravitational probes of dark matter physics, Phys. Rep. **761**, 1 (2018).

[6] D. Crnojević and B. Mutlu-Pakdil, Dwarf galaxies yesterday, now and tomorrow, Nat. Astron. **5**, 1191 (2021).

[7] L. V. Sales, A. Wetzel, and A. Fattahi, Baryonic solutions and challenges for cosmological models of dwarf galaxies, Nat. Astron. **6**, 897 (2022).

[8] S. Tulin and H.-B. Yu, Dark matter self-interactions and small scale structure, Phys. Rep. **730**, 1 (2018).

[9] S. Dodelson and L. M. Widrow, Sterile-neutrinos as dark matter, Phys. Rev. Lett. **72**, 17 (1994).

[10] J. R. Ellis, J. S. Hagelin, D. V. Nanopoulos, K. A. Olive, and M. Srednicki, Supersymmetric relics from the big bang, Nucl. Phys. **B238**, 453 (1984).

[11] W. Hu, R. Barkana, and A. Gruzinov, Cold and fuzzy dark matter, Phys. Rev. Lett. **85**, 1158 (2000).

[12] A. M. Brooks, Understanding dwarf galaxies in order to understand dark matter, in *Illuminating Dark Matter*, edited by R. Essig, J. Feng, and K. Zurek, Astrophysics and Space Science Proceedings Vol. 56 (Springer, New York, 2019), p. 19, arXiv:1812.00044.

[13] E. J. Tollerud, J. S. Bullock, L. E. Strigari, and B. Willman, Hundreds of Milky Way satellites? Luminosity bias in the satellite luminosity function, Astrophys. J. **688**, 277 (2008).

[14] S. Horiuchi, P. J. Humphrey, J. Onorbe, K. N. Abazajian, M. Kaplinghat, and S. Garrison-Kimmel, Sterile neutrino dark matter bounds from galaxies of the local group, Phys. Rev. D **89**, 025017 (2014).

[15] R. Kennedy, C. Frenk, S. Cole, and A. Benson, Constraining the warm dark matter particle mass with Milky Way satellites, Mon. Not. R. Astron. Soc. **442**, 2487 (2014).

[16] S. Y. Kim, A. H. G. Peter, and J. R. Hargis, Missing satellites problem: Completeness corrections to the number of satellite galaxies in the Milky Way are consistent with cold dark matter predictions, Phys. Rev. Lett. **121**, 211302 (2018).

[17] P. Jethwa, D. Erkal, and V. Belokurov, The upper bound on the lowest mass halo, Mon. Not. R. Astron. Soc. **473**, 2060 (2018).

[18] E. O. Nadler *et al.* (DES Collaboration), Milky Way satellite census. III. Constraints on dark matter properties from observations of Milky Way satellite galaxies, Phys. Rev. Lett. **126**, 091101 (2021).

[19] A. Dekker, S. Ando, C. A. Correa, and K. C. Y. Ng, Warm dark matter constraints using Milky Way satellite observations and subhalo evolution modeling, Phys. Rev. D **106**, 123026 (2022).

[20] S. Mau *et al.* (DES Collaboration), Milky Way satellite census. IV. Constraints on decaying dark matter from observations of Milky Way satellite galaxies, Astrophys. J. **932**, 128 (2022).

[21] K. Akita and S. Ando, Constraints on dark matter-neutrino scattering from the Milky-Way satellites and subhalo modeling for dark acoustic oscillations, J. Cosmol. Astropart. Phys. 11 (2023) 037.

[22] S. Y. Kim and A. H. G. Peter, The Milky Way satellite velocity function is a sharp probe of small-scale structure problems, arXiv:2106.09050.

[23] K. Subramanian, The origin, evolution and signatures of primordial magnetic fields, Rep. Prog. Phys. **79**, 076901 (2016).

[24] A. Achúcarro *et al.*, Inflation: Theory and observations, arXiv:2203.08128.

[25] P. W. Graham, J. Mardon, and S. Rajendran, Vector dark matter from inflationary fluctuations, Phys. Rev. D **93**, 103520 (2016).

[26] G. Alonso-Álvarez and J. Jaeckel, Lightish but clumpy: Scalar dark matter from inflationary fluctuations, J. Cosmol. Astropart. Phys. 10 (2018) 022.

[27] T. Tenkanen, Dark matter from scalar field fluctuations, Phys. Rev. Lett. **123**, 061302 (2019).

[28] A. R. Zentner and J. S. Bullock, Inflation, cold dark matter, and the central density problem, Phys. Rev. D **66**, 043003 (2002).

[29] A. R. Zentner and J. S. Bullock, Halo substructure and the power spectrum, Astrophys. J. **598**, 49 (2003).

[30] D. Gilman, A. Benson, J. Bovy, S. Birrer, T. Treu, and A. Nierenberg, The primordial matter power spectrum on subgalactic scales, Mon. Not. R. Astron. Soc. **512**, 3163 (2022).

[31] M. Kamionkowski and A. R. Liddle, The dearth of halo dwarf galaxies: Is there power on short scales?, Phys. Rev. Lett. **84**, 4525 (2000).

[32] N. Sabti, J. B. Muñoz, and D. Blas, New roads to the small-scale universe: Measurements of the clustering of matter with the high-redshift UV galaxy luminosity function, Astrophys. J. Lett. **928**, L20 (2022).

[33] https://github.com/garrett361/cmbpy.

[34] N. Dalal and C. S. Kochanek, Direct detection of CDM substructure, Astrophys. J. **572**, 25 (2002).

[35] A. S. Graus, J. S. Bullock, T. Kelley, M. Boylan-Kolchin, S. Garrison-Kimmel, and Y. Qi, How low does it go? Too few Galactic satellites with standard reionization quenching, Mon. Not. R. Astron. Soc. **488**, 4585 (2019).

[36] A. J. Benson, Galacticus: A semi-analytic model of galaxy formation, New Astron. **17**, 175 (2012).

[37] M. Rocha, A. H. G. Peter, and J. S. Bullock, Infall times for Milky Way satellites from their present-day kinematics, Mon. Not. R. Astron. Soc. **425**, 231 (2012).

[38] G. A. Dooley, A. H. G. Peter, T. Yang, B. Willman, B. F. Griffen, and A. Frebel, An observer's guide to the (local group) dwarf galaxies: Predictions for their own dwarf satellite populations, Mon. Not. R. Astron. Soc. **471**, 4894 (2017).

[39] S. P. Fillingham, M. C. Cooper, T. Kelley, M. K. Rodriguez Wimberly, M. Boylan-Kolchin, J. S. Bullock, S. Garrison-Kimmel, M. S. Pawlowski, and C. Wheeler, Characterizing the infall times and quenching timescales of Milky Way satellites with *Gaia* proper motions, arXiv:1906.04180.
[40] M. Cautun, A. Benitez-Llambay, A. J. Deason, C. S. Frenk, A. Fattahi, F. A. Gómez, R. J. J. Grand, K. A. Oman, J. F. Navarro, and C. M. Simpson, The Milky Way total mass profile as inferred from Gaia DR2, Mon. Not. R. Astron. Soc. **494**, 4291 (2020).
[41] W. H. Press and P. Schechter, Formation of galaxies and clusters of galaxies by self-similar gravitational condensation, Astrophys. J. **187**, 425 (1974).
[42] J. R. Bond, S. Cole, G. Efstathiou, and N. Kaiser, Excursion set mass functions for hierarchical Gaussian fluctuations, Astrophys. J. **379**, 440 (1991).
[43] J. L. Tinker, A. V. Kravtsov, A. Klypin, K. Abazajian, M. S. Warren, G. Yepes, S. Gottlober, and D. E. Holz, Toward a halo mass function for precision cosmology: The limits of universality, Astrophys. J. **688**, 709 (2008).
[44] A. J. Benson, A. Farahi, S. Cole, L. A. Moustakas, A. Jenkins, M. Lovell, R. Kennedy, J. Helly, and C. Frenk, Dark matter halo merger histories beyond cold dark matter: I—Methods and application to warm dark matter, Mon. Not. R. Astron. Soc. **428**, 1774 (2013).
[45] M. Leo, C. M. Baugh, B. Li, and S. Pascoli, A new smooth-*k* space filter approach to calculate halo abundances, J. Cosmol. Astropart. Phys. 04 (2018) 010.
[46] R. K. Sheth and G. Tormen, An excursion set model of hierarchical clustering: Ellipsoidal collapse and the moving barrier, Mon. Not. R. Astron. Soc. **329**, 61 (2002).
[47] A. Schneider, R. E. Smith, and D. Reed, Halo mass function and the free streaming scale, Mon. Not. R. Astron. Soc. **433**, 1573 (2013).
[48] S. Hirano, N. Zhu, N. Yoshida, D. Spergel, and H. W. Yorke, Early structure formation from primordial density fluctuations with a blue-tilted power spectrum, Astrophys. J. **814**, 18 (2015).
[49] S. Hirano and N. Yoshida, Early structure formation from primordial density fluctuations with a blue, tilted power spectrum—II. High-redshift galaxies, Astrophys. J. **963**, 2 (2024).
[50] S. Bohr, J. Zavala, F.-Y. Cyr-Racine, and M. Vogelsberger, The halo mass function and inner structure of ETHOS haloes at high redshift, Mon. Not. R. Astron. Soc. **506**, 128 (2021).
[51] A. J. Benson, A. Ludlow, and S. Cole, Halo concentrations from extended Press-Schechter merger histories, Mon. Not. R. Astron. Soc. **485**, 5010 (2019).
[52] S. Cole, C. G. Lacey, C. M. Baugh, and C. S. Frenk, Hierarchical galaxy formation, Mon. Not. R. Astron. Soc. **319**, 168 (2000).
[53] H. Parkinson, S. Cole, and J. Helly, Generating dark matter halo merger trees, Mon. Not. R. Astron. Soc. **383**, 557 (2008).
[54] R. K. Sheth, H. J. Mo, and G. Tormen, Ellipsoidal collapse and an improved model for the number and spatial distribution of dark matter haloes, Mon. Not. R. Astron. Soc. **323**, 1 (2001).
[55] S. Garrison-Kimmel *et al.*, Not so lumpy after all: Modelling the depletion of dark matter subhaloes by Milky Way-like galaxies, Mon. Not. R. Astron. Soc. **471**, 1709 (2017).
[56] A. J. Benson, The normalization and slope of the dark matter (sub-)halo mass function on sub-galactic scales, Mon. Not. R. Astron. Soc. **493**, 1268 (2020).
[57] J. Richings *et al.*, Subhalo destruction in the APOSTLE and AURIGA simulations, Mon. Not. R. Astron. Soc. **492**, 5780 (2020).
[58] J. Samuel *et al.*, A profile in FIRE: Resolving the radial distributions of satellite galaxies in the local group with simulations, Mon. Not. R. Astron. Soc. **491**, 1471 (2020).
[59] J. F. Navarro, C. S. Frenk, and S. D. M. White, A universal density profile from hierarchical clustering, Astrophys. J. **490**, 493 (1997).
[60] R. H. Wechsler, J. S. Bullock, J. R. Primack, A. V. Kravtsov, and A. Dekel, Concentrations of dark halos from their assembly histories, Astrophys. J. **568**, 52 (2002).
[61] A. D. Ludlow, S. Bose, R. E. Angulo, L. Wang, W. A. Hellwing, J. F. Navarro, S. Cole, and C. S. Frenk, The mass–concentration–redshift relation of cold and warm dark matter haloes, Mon. Not. R. Astron. Soc. **460**, 1214 (2016).
[62] B. Diemer and M. Joyce, An accurate physical model for halo concentrations, Astrophys. J. **871**, 168 (2019).
[63] J. Wang, S. Bose, C. S. Frenk, L. Gao, A. Jenkins, V. Springel, and S. D. M. White, Universal structure of dark matter haloes over a mass range of 20 orders of magnitude, Nature (London) **585**, 39 (2020).
[64] B. Diemer and A. V. Kravtsov, A universal model for halo concentrations, Astrophys. J. **799**, 108 (2015).
[65] C. G. Lacey and S. Cole, Merger rates in hierarchical models of galaxy formation, Mon. Not. R. Astron. Soc. **262**, 627 (1993).
[66] S. Dodelson, *Modern Cosmology* (Academic Press, Amsterdam, 2003).
[67] https://github.com/stacykim/disSat.
[68] A. J. Deason, A. R. Wetzel, S. Garrison-Kimmel, and V. Belokurov, Satellites of LMC-mass dwarfs: Close friendships ruined by Milky Way mass haloes, Mon. Not. R. Astron. Soc. **453**, 3568 (2015).
[69] M. Barry, A. Wetzel, S. Chapman, J. Samuel, R. Sanderson, and A. Arora, The dark side of FIRE: Predicting the population of dark matter subhaloes around Milky Way-mass galaxies, Mon. Not. R. Astron. Soc. **523**, 428 (2023).
[70] R. D'Souza and E. F. Bell, The infall of dwarf satellite galaxies are influenced by their host's massive accretions, Mon. Not. R. Astron. Soc. **504**, 5270 (2021).
[71] E. O. Nadler *et al.* (DES Collaboration), Milky Way satellite census—II. Galaxy-halo connection constraints including the impact of the Large Magellanic Cloud, Astrophys. J. **893**, 48 (2020).
[72] E. O. Nadler, A. Banerjee, S. Adhikari, Y.-Y. Mao, and R. H. Wechsler, The effects of dark matter and baryonic physics on the Milky Way subhalo population in the presence of the Large Magellanic Cloud, Astrophys. J. Lett. **920**, L11 (2021).

[73] V. Manwadkar and A. V. Kravtsov, Forward-modelling the luminosity, distance, and size distributions of the Milky Way satellites, Mon. Not. R. Astron. Soc. **516**, 3944 (2022).
[74] B. C. Conn, H. Jerjen, D. Kim, and M. Schirmer, On the nature of ultra-faint dwarf galaxy candidates. I. DES1, Eridanus III, and Tucana V, Astrophys. J. **852**, 68 (2018).
[75] B. C. Conn, H. Jerjen, D. Kim, and M. Schirmer, On the nature of ultra-faint dwarf galaxy candidates. II. The case of Cetus II, Astrophys. J. **857**, 70 (2018).
[76] H. Jerjen, B. Conn, D. Kim, and M. Schirmer, On the nature of ultra-faint dwarf galaxy candidates. III. Horologium I, Pictor I, Grus I, and Phoenix II, arXiv:1809.02259.
[77] B. Mutlu-Pakdil, D. J. Sand, J. L. Carlin, K. Spekkens, N. Caldwell, D. Crnojević, A. K. Hughes, B. Willman, and D. Zaritsky, A deeper look at the new Milky Way satellites: Sagittarius II, Reticulum II, Phoenix II, and Tucana III, Astrophys. J. **863**, 25 (2018).
[78] S. A. Cantu *et al.* (DES Collaboration), A deeper look at DES dwarf galaxy candidates: Grus I and Indus II, Astrophys. J. **916**, 81 (2021).
[79] S. Mau *et al.* (DELVE Collaboration), Two ultra-faint Milky Way stellar systems discovered in early data from the DECam local volume exploration survey, Astrophys. J. **890**, 136 (2020).
[80] C. E. Martínez-Vázquez *et al.* (DELVE Collaboration), RR Lyrae stars in the newly discovered ultra-faint dwarf galaxy Centaurus I*, Astron. J. **162**, 253 (2021).
[81] W. Cerny *et al.* (DELVE Collaboration), Eridanus IV: An ultra-faint dwarf galaxy candidate discovered in the DECam local volume exploration survey, Astrophys. J. Lett. **920**, L44 (2021).
[82] W. Cerny *et al.* (DELVE Collaboration), Pegasus IV: Discovery and spectroscopic confirmation of an ultra-faint dwarf galaxy in the constellation pegasus, Astrophys. J. **942**, 111 (2023).
[83] W. Cerny *et al.* (DELVE Collaboration), Six more ultra-faint Milky Way companions discovered in the DECam local volume exploration survey, Astrophys. J. **953**, 1 (2023).
[84] G. Torrealba *et al.*, Discovery of two neighbouring satellites in the Carina constellation with MagLiteS, Mon. Not. R. Astron. Soc. **475**, 5085 (2018).
[85] P. Jethwa, D. Erkal, and V. Belokurov, A magellanic origin of the DES dwarfs, Mon. Not. R. Astron. Soc. **461**, 2212 (2016).
[86] N. Garavito-Camargo, E. Patel, G. Besla, A. M. Price-Whelan, F. A. Gómez, C. F. P. Laporte, and K. V. Johnston, The clustering of orbital poles induced by the LMC: Hints for the origin of planes of satellites, Astrophys. J. **923**, 140 (2021).
[87] S. Vegetti, L. V. E. Koopmans, M. W. Auger, T. Treu, and A. S. Bolton, Inference of the cold dark matter substructure mass function at $z = 0.2$ using strong gravitational lenses, Mon. Not. R. Astron. Soc. **442**, 2017 (2014).
[88] K. T. Inoue, R. Takahashi, T. Takahashi, and T. Ishiyama, Constraints on warm dark matter from weak lensing in anomalous quadruple lenses, Mon. Not. R. Astron. Soc. **448**, 2704 (2015).
[89] Y. D. Hezaveh *et al.*, Detection of lensing substructure using ALMA observations of the dusty galaxy SDP.81, Astrophys. J. **823**, 37 (2016).
[90] S. Birrer, A. Amara, and A. Refregier, Lensing substructure quantification in RXJ1131-1231: A 2 keV lower bound on dark matter thermal relic mass, J. Cosmol. Astropart. Phys. 05 (2017) 037.
[91] D. Gilman, S. Birrer, A. Nierenberg, T. Treu, X. Du, and A. Benson, Warm dark matter chills out: Constraints on the halo mass function and the free-streaming length of dark matter with eight quadruple-image strong gravitational lenses, Mon. Not. R. Astron. Soc. **491**, 6077 (2020).
[92] J.-W. Hsueh, W. Enzi, S. Vegetti, M. Auger, C. D. Fassnacht, G. Despali, L. V. E. Koopmans, and J. P. McKean, SHARP—VII. New constraints on the dark matter free-streaming properties and substructure abundance from gravitationally lensed quasars, Mon. Not. R. Astron. Soc. **492**, 3047 (2020).
[93] P. J. Quinn, L. Hernquist, and D. P. Fullagar, Heating of galactic disks by mergers, Astrophys. J. **403**, 74 (1993).
[94] R. Feldmann and D. Spolyar, Detecting dark matter substructures around the Milky Way with Gaia, Mon. Not. R. Astron. Soc. **446**, 1000 (2015).
[95] J. H. Yoon, K. V. Johnston, and D. W. Hogg, Clumpy streams from clumpy halos: Detecting missing satellites with cold stellar structures, Astrophys. J. **731**, 58 (2011).
[96] R. G. Carlberg, Dark matter sub-halo counts via star stream crossings, Astrophys. J. **748**, 20 (2012).
[97] C. Aganze, S. Pearson, T. Starkenburg, G. Contardo, K. V. Johnston, K. Tavangar, A. M. Price-Whelan, and A. J. Burgasser, Prospects for detecting gaps in globular cluster stellar streams in external galaxies with the Nancy Grace Roman Space Telescope, Astrophys. J. **962**, 151 (2024).
[98] E. J. Tollerud, J. S. Bullock, G. J. Graves, and J. Wolf, From galaxy clusters to ultra-faint dwarf spheroidals: A fundamental curve connecting dispersion-supported galaxies to their dark matter halos, Astrophys. J. **726**, 108 (2011).
[99] L. E. Strigari, J. S. Bullock, M. Kaplinghat, J. D. Simon, M. Geha, B. Willman, and M. G. Walker, A common mass scale for satellite galaxies of the Milky Way, Nature (London) **454**, 1096 (2008).
[100] A. W. McConnachie, The observed properties of dwarf galaxies in and around the local group, Astron. J. **144**, 4 (2012).
[101] J. I. Read, G. Iorio, O. Agertz, and F. Fraternali, The stellar mass–halo mass relation of isolated field dwarfs: A critical test of ΛCDM at the edge of galaxy formation, Mon. Not. R. Astron. Soc. **467**, 2019 (2017).
[102] S. Danieli, P. van Dokkum, and C. Conroy, Hunting faint dwarf galaxies in the field using integrated light surveys, Astrophys. J. **856**, 69 (2018).
[103] F. Jiang *et al.*, Is the dark-matter halo spin a predictor of galaxy spin and size?, Mon. Not. R. Astron. Soc. **488**, 4801 (2019).
[104] B. P. Moster, T. Naab, and S. D. M. White, Galactic star formation and accretion histories from matching galaxies to dark matter haloes, Mon. Not. R. Astron. Soc. **428**, 3121 (2013).

[105] R. H. Wechsler and J. L. Tinker, The connection between galaxies and their dark matter halos, Annu. Rev. Astron. Astrophys. **56**, 435 (2018).
[106] F. Munshi, A. M. Brooks, E. Applebaum, C. R. Christensen, T. Quinn, and S. Sligh, Quantifying scatter in galaxy formation at the lowest masses, Astrophys. J. **923**, 35 (2021).
[107] D. Zaritsky and P. Behroozi, Photometric mass estimation and the stellar mass-halo mass relation for low mass galaxies, Mon. Not. R. Astron. Soc. **519**, 871 (2023).
[108] S. Garrison-Kimmel, J. S. Bullock, M. Boylan-Kolchin, and E. Bardwell, Organized chaos: Scatter in the relation between stellar mass and halo mass in small galaxies, Mon. Not. R. Astron. Soc. **464**, 3108 (2017).
[109] T. Buck, A. V. Macciò, A. A. Dutton, A. Obreja, and J. Frings, NIHAO XV: The environmental impact of the host galaxy on galactic satellite and field dwarf galaxies, Mon. Not. R. Astron. Soc. **483**, 1314 (2019).
[110] R. J. J. Grand, F. Marinacci, R. Pakmor, C. M. Simpson, A. J. Kelly, F. A. Gómez, A. Jenkins, V. Springel, C. S. Frenk, and S. D. M. White, Determining the full satellite population of a Milky Way-mass halo in a highly resolved cosmological hydrodynamic simulation, Mon. Not. R. Astron. Soc. **507**, 4953 (2021).
[111] J. Wolf, G. D. Martinez, J. S. Bullock, M. Kaplinghat, M. Geha, R. R. Munoz, J. D. Simon, and F. F. Avedo, Accurate masses for dispersion-supported galaxies, Mon. Not. R. Astron. Soc. **406**, 1220 (2010).
[112] J. I. Read and G. Gilmore, Mass loss from dwarf spheroidal galaxies: The origins of shallow dark matter cores and exponential surface brightness profiles, Mon. Not. R. Astron. Soc. **356**, 107 (2005).
[113] R. Leaman, K. A. Venn, A. M. Brooks, G. Battaglia, A. A. Cole, R. A. Ibata, M. J. Irwin, A. W. McConnachie, J. T. Mendel, and E. Tolstoy, The resolved structure and dynamics of an isolated dwarf galaxy: A VLT and Keck spectroscopic survey of WLM, Astrophys. J. **750**, 33 (2012).
[114] D. R. Weisz *et al.*, Modeling the effects of star formation histories on halpha and ultra-violet fluxes in nearby dwarf galaxies, Astrophys. J. **744**, 44 (2012).
[115] F. Governato, A. Zolotov, A. Pontzen, C. Christensen, S. H. Oh, A. M. Brooks, T. Quinn, S. Shen, and J. Wadsley, Cuspy no more: How outflows affect the central dark matter and baryon distribution in Λ cold dark matter galaxies, Mon. Not. R. Astron. Soc. **422**, 1231 (2012).
[116] R. Teyssier, A. Pontzen, Y. Dubois, and J. Read, Cusp-core transformations in dwarf galaxies: Observational predictions, Mon. Not. R. Astron. Soc. **429**, 3068 (2013).
[117] A. Di Cintio, C. B. Brook, A. V. Macciò, G. S. Stinson, A. Knebe, A. A. Dutton, and J. Wadsley, The dependence of dark matter profiles on the stellar-to-halo mass ratio: A prediction for cusps versus cores, Mon. Not. R. Astron. Soc. **437**, 415 (2014).
[118] G. Kauffmann, Quantitative constraints on starburst cycles in galaxies with stellar masses in the range $10^8 - 10^{10} M_\odot$, Mon. Not. R. Astron. Soc. **441**, 2717 (2014).
[119] K. B. W. McQuinn, F. Lelli, E. D. Skillman, A. E. Dolphin, S. S. McGaugh, and B. F. Williams, The link between mass distribution and starbursts in dwarf galaxies, Mon. Not. R. Astron. Soc. **450**, 3886 (2015).
[120] J. Peñarrubia, A. Pontzen, M. G. Walker, and S. E. Koposov, The coupling between the core/cusp and missing satellite problems, Astrophys. J. Lett. **759**, L42 (2012).
[121] R. Errani, J. F. Navarro, J. Peñarrubia, B. Famaey, and R. Ibata, Dark matter halo cores and the tidal survival of Milky Way satellites, Mon. Not. R. Astron. Soc. **519**, 384 (2022).
[122] A. Di Cintio, C. B. Brook, A. V. Macciò, G. S. Stinson, A. Knebe, A. A. Dutton, and J. Wadsley, The dependence of dark matter profiles on the stellar-to-halo mass ratio: A prediction for cusps versus cores, Mon. Not. R. Astron. Soc. **437**, 415 (2014).
[123] S. Bose *et al.*, No cores in dark matter-dominated dwarf galaxies with bursty star formation histories, Mon. Not. R. Astron. Soc. **486**, 4790 (2019).
[124] J. I. Read, O. Agertz, and M. L. M. Collins, Dark matter cores all the way down, Mon. Not. R. Astron. Soc. **459**, 2573 (2016).
[125] E. A. Baltz, P. Marshall, and M. Oguri, Analytic models of plausible gravitational lens potentials, J. Cosmol. Astropart. Phys. 01 (2009) 015.
[126] I. King, The structure of star clusters. I. An empirical density law, Astron. J. **67**, 471 (1962).
[127] O. Y. Gnedin, L. Hernquist, and J. P. Ostriker, Tidal shocking by extended mass distributions, Astrophys. J. **514**, 109 (1999).
[128] J. I. Read, M. I. Wilkinson, N. W. Evans, G. Gilmore, and J. T. Kleyna, The tidal stripping of satellites, Mon. Not. R. Astron. Soc. **366**, 429 (2006).
[129] G. A. Dooley, A. H. G. Peter, M. Vogelsberger, J. Zavala, and A. Frebel, Enhanced tidal stripping of satellites in the galactic halo from dark matter self-interactions, Mon. Not. R. Astron. Soc. **461**, 710 (2016).
[130] M. S. Delos, Tidal evolution of dark matter annihilation rates in subhalos, Phys. Rev. D **100**, 063505 (2019).
[131] N. E. Drakos, J. E. Taylor, and A. J. Benson, Mass loss in tidally stripped systems; the energy-based truncation method, Mon. Not. R. Astron. Soc. **494**, 378 (2020).
[132] J. Penarrubia, A. J. Benson, M. G. Walker, G. Gilmore, A. McConnachie, and L. Mayer, The impact of dark matter cusps and cores on the satellite galaxy population around spiral galaxies, Mon. Not. R. Astron. Soc. **406**, 1290 (2010).
[133] R. Errani and J. F. Navarro, The asymptotic tidal remnants of cold dark matter subhaloes, Mon. Not. R. Astron. Soc. **505**, 18 (2021).
[134] A. J. Benson and X. Du, Tidal tracks and artificial disruption of cold dark matter haloes, Mon. Not. R. Astron. Soc. **517**, 1398 (2022).
[135] S. Garrison-Kimmel, M. Boylan-Kolchin, J. Bullock, and K. Lee, ELVIS: Exploring the local volume in simulations, Mon. Not. R. Astron. Soc. **438**, 2578 (2014).
[136] J. D. Simon, The faintest dwarf galaxies, Annu. Rev. Astron. Astrophys. **57**, 375 (2019).
[137] S. Weerasooriya, M. S. Bovill, A. Benson, A. M. Musick, and M. Ricotti, Devouring the Milky Way satellites: Modeling dwarf galaxies with galacticus, Astrophys. J. **948**, 87 (2023).

[138] I. M. E. Santos-Santos, L. V. Sales, A. Fattahi, and J. F. Navarro, Satellite mass functions and the faint end of the galaxy mass–halo mass relation in LCDM, Mon. Not. R. Astron. Soc. **515**, 3685 (2022).
[139] J. L. Sanders, N. W. Evans, and W. Dehnen, Tidal disruption of dwarf spheroidal galaxies: The strange case of Crater II, Mon. Not. R. Astron. Soc. **478**, 3879 (2018).
[140] R. Errani, J. F. Navarro, R. Ibata, and J. Peñarrubia, Structure and kinematics of tidally limited satellite galaxies in LCDM, Mon. Not. R. Astron. Soc. **511**, 6001 (2022).
[141] L. Dai and J. Miralda-Escudé, Gravitational lensing signatures of axion dark matter minihalos in highly magnified stars, Astron. J. **159**, 49 (2020).
[142] R. Lunnan, M. Vogelsberger, A. Frebel, L. Hernquist, A. Lidz, and M. Boylan-Kolchin, The effects of patchy reionization on satellite galaxies of the Milky Way, Astrophys. J. **746**, 109 (2012).
[143] D. Koh and J. H. Wise, Extending semi-numeric reionization models to the first stars and galaxies, Mon. Not. R. Astron. Soc. **474**, 3817 (2018).
[144] M. P. Rey, A. Pontzen, O. Agertz, M. D. A. Orkney, J. I. Read, A. Saintonge, and C. Pedersen, EDGE: The origin of scatter in ultra-faint dwarf stellar masses and surface brightnesses, Astrophys. J. Lett. **886**, L3 (2019).
[145] C. Barber, E. Starkenburg, J. Navarro, A. McConnachie, and A. Fattahi, The orbital ellipticity of satellite galaxies and the mass of the Milky Way, Mon. Not. R. Astron. Soc. **437**, 959 (2014).
[146] J. Woo, S. Courteau, and A. Dekel, Scaling relations and the fundamental line of the local group dwarf galaxies, Mon. Not. R. Astron. Soc. **390**, 1453 (2008).
[147] S. Koposov *et al.*, The luminosity function of the Milky Way satellites, Astrophys. J. **686**, 279 (2008).
[148] S. Walsh, B. Willman, and H. Jerjen, The invisibles: A detection algorithm to trace the faintest Milky Way satellites, Astron. J. **137**, 450 (2009).
[149] S. Garrison-Kimmel *et al.*, Not so lumpy after all: Modelling the depletion of dark matter subhaloes by Milky Way-like galaxies, Mon. Not. R. Astron. Soc. **471**, 1709 (2017).
[150] O. Y. Gnedin, A. V. Kravtsov, A. A. Klypin, and D. Nagai, Response of dark matter halos to condensation of baryons: Cosmological simulations and improved adiabatic contraction model, Astrophys. J. **616**, 16 (2004).
[151] M. G. Abadi, J. F. Navarro, M. Fardal, A. Babul, and M. Steinmetz, Galaxy-induced transformation of dark matter halos, Mon. Not. R. Astron. Soc. **407**, 435 (2010).
[152] E. D'Onghia, V. Springel, L. Hernquist, and D. Keres, Substructure depletion in the Milky Way halo by the disk, Astrophys. J. **709**, 1138 (2010).
[153] A. M. Brooks, M. Kuhlen, A. Zolotov, and D. Hooper, A baryonic solution to the missing satellites problem, Astrophys. J. **765**, 22 (2013).
[154] T. Sawala, P. Pihajoki, P. H. Johansson, C. S. Frenk, J. F. Navarro, K. A. Oman, and S. D. M. White, Shaken and stirred: The Milky Way's dark substructures, Mon. Not. R. Astron. Soc. **467**, 4383 (2017).
[155] A. B. Pace, D. Erkal, and T. S. Li, Proper motions, orbits, and tidal influences of Milky Way dwarf spheroidal galaxies, Astrophys. J. **940**, 136 (2022).
[156] E. N. Kirby, M. Boylan-Kolchin, J. G. Cohen, M. Geha, J. S. Bullock, and M. Kaplinghat, Segue 2: The least massive galaxy, Astrophys. J. **770**, 16 (2013).
[157] N. Aghanim *et al.* (Planck Collaboration), Planck 2018 results. I. Overview and the cosmological legacy of Planck, Astron. Astrophys. **641**, A1 (2020).
[158] M. A. Troxel *et al.* (DES Collaboration), Dark Energy Survey Year 1 results: Cosmological constraints from cosmic shear, Phys. Rev. D **98**, 043528 (2018).
[159] S. Chabanier, M. Millea, and N. Palanque-Delabrouille, Matter power spectrum: From Lyα forest to CMB scales, Mon. Not. R. Astron. Soc. **489**, 2247 (2019).
[160] https://github.com/marius311/mpk_compilation.
[161] M. Sten Delos, T. Linden, and A. L. Erickcek, Breaking a dark degeneracy: The gamma-ray signature of early matter domination, Phys. Rev. D **100**, 123546 (2019).
[162] M. S. Delos, K. Redmond, and A. L. Erickcek, How an era of kination impacts substructure and the dark matter annihilation rate, Phys. Rev. D **108**, 023528 (2023).
[163] A. Kravtsov and V. Manwadkar, GRUMPY: A simple framework for realistic forward modelling of dwarf galaxies, Mon. Not. R. Astron. Soc. **514**, 2667 (2022).
[164] S. Kim *et al.*, EDGE: Predictable scatter in the stellar mass–halo mass relation of dwarf galaxies, arXiv:2408.15214.
[165] A. Kravtsov and Z. Wu, Densities and mass assembly histories of the Milky Way satellites are not a challenge to ΛCDM, Mon. Not. R. Astron. Soc. **525**, 325 (2023).
[166] A. Drlica-Wagner, L. J. Kewley, J. R. Rigby, A. Acharyya, D. A. Berg, M. Bayliss, and K. Sharon (DES Collaboration), Milky Way satellite census. I. The observational selection function for Milky Way satellites in DES Y3 and Pan-STARRS DR1, Astrophys. J. **893**, 1 (2020).
[167] P. A. Abell *et al.* (LSST Science, LSST Project Collaborations), LSST science book, version 2.0, arXiv:0912.0201.
[168] B. Mutlu-Pakdıl, D. J. Sand, D. Crnojević, A. Drlica-Wagner, N. Caldwell, P. Guhathakurta, A. C. Seth, J. D. Simon, J. Strader, and E. Toloba, Resolved dwarf galaxy searches within ∼5 Mpc with the Vera Rubin Observatory and Subaru Hyper Suprime-Cam, Astrophys. J. **918**, 88 (2021).
[169] R. Adam *et al.* (Planck Collaboration), Planck intermediate results. XLVII. Planck constraints on reionization history, Astron. Astrophys. **596**, A108 (2016).
[170] M. Castellano, N. Menci, and M. Romanello, Constraints on dark matter from reionization, Frascati Phys. Ser. **74**, 209 (2022).
[171] S. R. Furlanetto, The 21-cm line as a probe of reionization, in *Understanding the Epoch of Cosmic Reionization* (Springer, Cham, 2016).
[172] R. P. Naidu *et al.*, Two remarkably luminous galaxy candidates at $z \approx 10 - 12$ revealed by JWST, Astrophys. J. Lett. **940**, L14 (2022).
[173] M. Castellano *et al.*, Early results from GLASS-JWST. III. Galaxy candidates at z 9-15, Astrophys. J. Lett. **938**, L15 (2022).
[174] M. Castellano *et al.*, Early results from GLASS-JWST. XIX. A high density of bright galaxies at $z \approx 10$ in the A2744 region, Astrophys. J. Lett. **948**, L14 (2023).

[175] N. J. Adams *et al.*, Discovery and properties of ultra-high redshift galaxies ($9 < z < 12$) in the JWST ERO SMACS 0723 Field, Mon. Not. R. Astron. Soc. **518**, 4755 (2023).
[176] H. Atek *et al.*, Revealing galaxy candidates out to z 16 with JWST observations of the lensing cluster SMACS0723, Mon. Not. R. Astron. Soc. **519**, 1201 (2023).
[177] F. R. Donnan, I. García-Bernete, D. Rigopoulou, M. Pereira-Santaella, A. Alonso-Herrero, P. F. Roche, A. Hernán-Caballero, and H. W. W. Spoon, The obscured nucleus and shocked environment of VV 114E revealed by JWST/MIRI spectroscopy, Mon. Not. R. Astron. Soc. **519**, 3691 (2023).
[178] C. T. Donnan, D. J. McLeod, R. J. McLure, J. S. Dunlop, A. C. Carnall, F. Cullen, and D. Magee, The abundance of $z \gtrsim 10$ galaxy candidates in the HUDF using deep JWST NIRCam medium-band imaging, Mon. Not. R. Astron. Soc. **520**, 4554 (2023).
[179] Y. Harikane, M. Ouchi, M. Oguri, Y. Ono, K. Nakajima, Y. Isobe, H. Umeda, K. Mawatari, and Y. Zhang, A comprehensive study of galaxies at z~9–16 found in the early JWST data: Ultraviolet luminosity functions and cosmic star formation history at the pre-reionization epoch, Astrophys. J. Suppl. Ser. **265**, 5 (2023).
[180] R. Bouwens, G. Illingworth, P. Oesch, M. Stefanon, R. Naidu, I. van Leeuwen, and D. Magee, UV luminosity density results at $z > 8$ from the first JWST/NIRCam fields: Limitations of early data sets and the need for spectroscopy, Mon. Not. R. Astron. Soc. **523**, 1009 (2023).
[181] R. J. Bouwens, M. Stefanon, G. Brammer, P. A. Oesch, T. Herard-Demanche, G. D. Illingworth, J. Matthee, R. P. Naidu, P. G. van Dokkum, and I. F. van Leeuwen, Evolution of the UV LF from z 15 to z 8 using new JWST NIRCam medium-band observations over the HUDF/XDF, Mon. Not. R. Astron. Soc. **523**, 1036 (2023).
[182] T. Morishita, Abdurro'uf, H. Hirashita, A. B. Newman, M. Stiavelli, and M. Chiaberge, Compact dust emission in a gravitationally lensed massive quiescent galaxy at $z = 2.15$ revealed in 130 pc resolution observations by the atacama large millimeter/submillimeter array, Astrophys. J. **938**, 144 (2022).
[183] Y. Harikane, K. Nakajima, M. Ouchi, H. Umeda, Y. Isobe, Y. Ono, Y. Xu, and Y. Zhang, Pure spectroscopic constraints on UV luminosity functions and cosmic star formation history from 25 galaxies at $z_{\rm spec} = 8.61$–13.20 confirmed with JWST/NIRSpec, arXiv:2304.06658.
[184] P. Dayal and S. K. Giri, Warm dark matter constraints from the JWST, Mon. Not. R. Astron. Soc. **528**, 2784 (2024).
[185] N. Menci, A. Grazian, M. Castellano, and N. G. Sanchez, A stringent limit on the warm dark matter particle masses from the abundance of $z = 6$ galaxies in the Hubble frontier fields, Astrophys. J. Lett. **825**, L1 (2016).
[186] N. Sabti, J. B. Muñoz, and M. Kamionkowski, Insights from HST into ultra-massive galaxies and early-universe cosmology, Phys. Rev. Lett. **132**, 061002 (2024).
[187] P. Parashari and R. Laha, Primordial power spectrum in light of JWST observations of high redshift galaxies, Mon. Not. R. Astron. Soc. **526**, L63 (2023).
[188] F. Zwicky, Die Rotverschiebung von extragalaktischen Nebeln, Helv. Phys. Acta **6**, 110 (1933).
[189] F. Zwicky, On the masses of nebulae and of clusters of nebulae, Astrophys. J. **86**, 217 (1937).
[190] E. Komatsu *et al.* (WMAP Collaboration), Five-Year Wilkinson Microwave Anisotropy Probe (WMAP) observations: Cosmological interpretation, Astrophys. J. Suppl. Ser. **180**, 330 (2009).
[191] A. R. Zentner, A. A. Berlind, J. S. Bullock, A. V. Kravtsov, and R. H. Wechsler, The physics of galaxy clustering. 1. A model for subhalo populations, Astrophys. J. **624**, 505 (2005).
[192] R. Errani, J. Peñarrubia, and M. G. Walker, Systematics in virial mass estimators for pressure-supported systems, Mon. Not. R. Astron. Soc. **481**, 5073 (2018).
[193] J. Einasto, On the construction of a composite model for the galaxy and on the determination of the system of galactic parameters, Tr. Astrofiz. Inst. Alma-Ata **5**, 87 (1965).
[194] https://www.cadc-ccda.hia-iha.nrc-cnrc.gc.ca/en/community/nearby/.
[195] E. O. Nadler, Y.-Y. Mao, G. M. Green, and R. H. Wechsler, Modeling the connection between subhalos and satellites in Milky Way–like systems, Astrophys. J. **873**, 34 (2019).
[196] M. Boylan-Kolchin, V. Springel, S. D. M. White, and A. Jenkins, There's no place like home? Statistics of Milky Way-mass dark matter halos, Mon. Not. R. Astron. Soc. **406**, 896 (2010).
[197] C. E. Fielder, Y.-Y. Mao, J. A. Newman, A. R. Zentner, and T. C. Licquia, Predictably missing satellites: Subhalo abundances in Milky Way-like haloes, Mon. Not. R. Astron. Soc. **486**, 4545 (2019).
[198] S. S. Wilks, The large-sample distribution of the likelihood ratio for testing composite hypotheses, Ann. Math. Stat. **9**, 60 (1938).
[199] G. P. Lepage, Adaptive multidimensional integration: VEGAS enhanced, J. Comput. Phys. **439**, 110386 (2021).
[200] M. J. D. Powell, The BOBYQA algorithm for bound constrained optimization without derivatives, Technical Report DAMTP 2009/NA06, University of Cambridge, 2009.
[201] C. Cartis, J. Fiala, B. Marteau, and L. Roberts, Improving the flexibility and robustness of model-based derivative-free optimization solvers, ACM Trans. Math. Softw. **45**, 41 (2019).
[202] V. Belokurov, M. G. Walker, N. W. Evans, G. Gilmore, M. J. Irwin, M. Mateo, L. Mayer, E. Olszewski, J. Bechtold, and T. Pickering, Segue 2: A prototype of the population of satellites of satellites, Mon. Not. R. Astron. Soc. **397**, 1748 (2009).